BT5441 – Term Project - Supplementary File *(Group 6)*

$$(IVC)_i = \frac{(VCD_i \cdot V_i) + (VCD_{i-2} \cdot V_{i-2})}{2}(t_i - t_{i-2})$$

Equation 1: Integral Viable Cell Computation

$$(S_{i-1})(V_{i-1} - D_{i-1}) + S_f F \quad \rightarrow \quad \text{Initial moles of } S$$

$$V_i(S_i) \quad \rightarrow \quad \text{Final moles of } S$$

$$(q_S)_i = \frac{1}{(IVC)_i}\{\text{Final moles of } S - \text{Initial moles of } S\}$$

$$S_{i-2} + \left(\frac{S_i - S_{i-2}}{t_i - t_{i-2}}\right)(t_{i-1} - t_{i-2}) = S_{i-1}$$

$$(q_S)_i = \frac{\left[(V_i S_i) - \left((S_{i-2}V_{i-2}) - \{(S_{i-2}D_{i-2}) + (S_{i-1}D_{i-1})\} + \{(S_f F)_{i-2} + (S_f F)_{i-1}\}\right)\right]}{(IVC)_i}$$

Equation 2: Specific Metabolic Rate Calculation Formula

(Linearly Interpolated Data for substrate concentration)

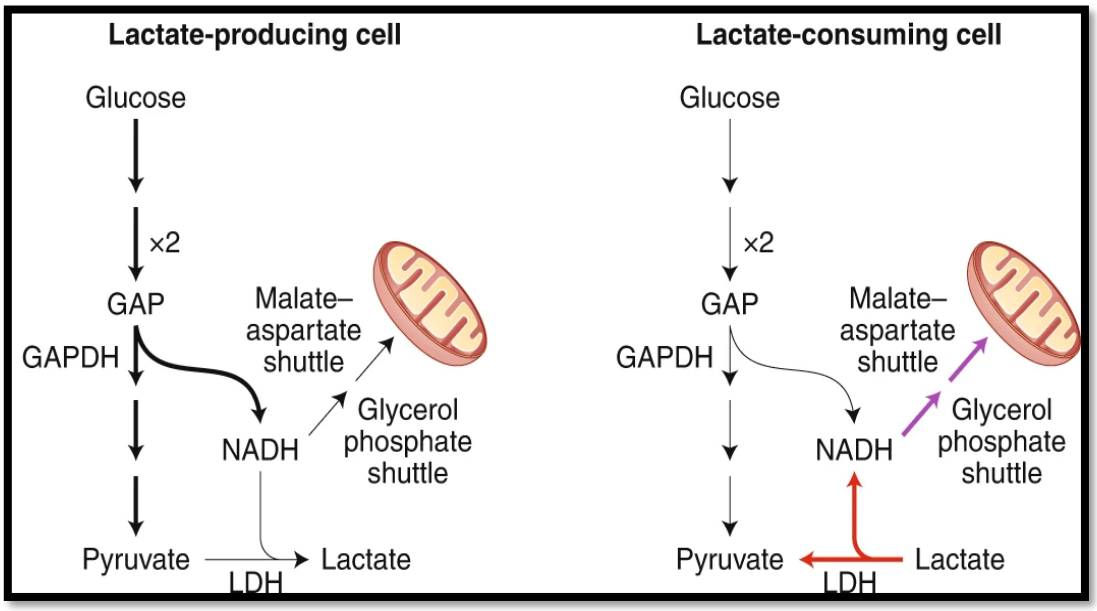

Figure 1: Reactions involved in Lactate Production and Consumption

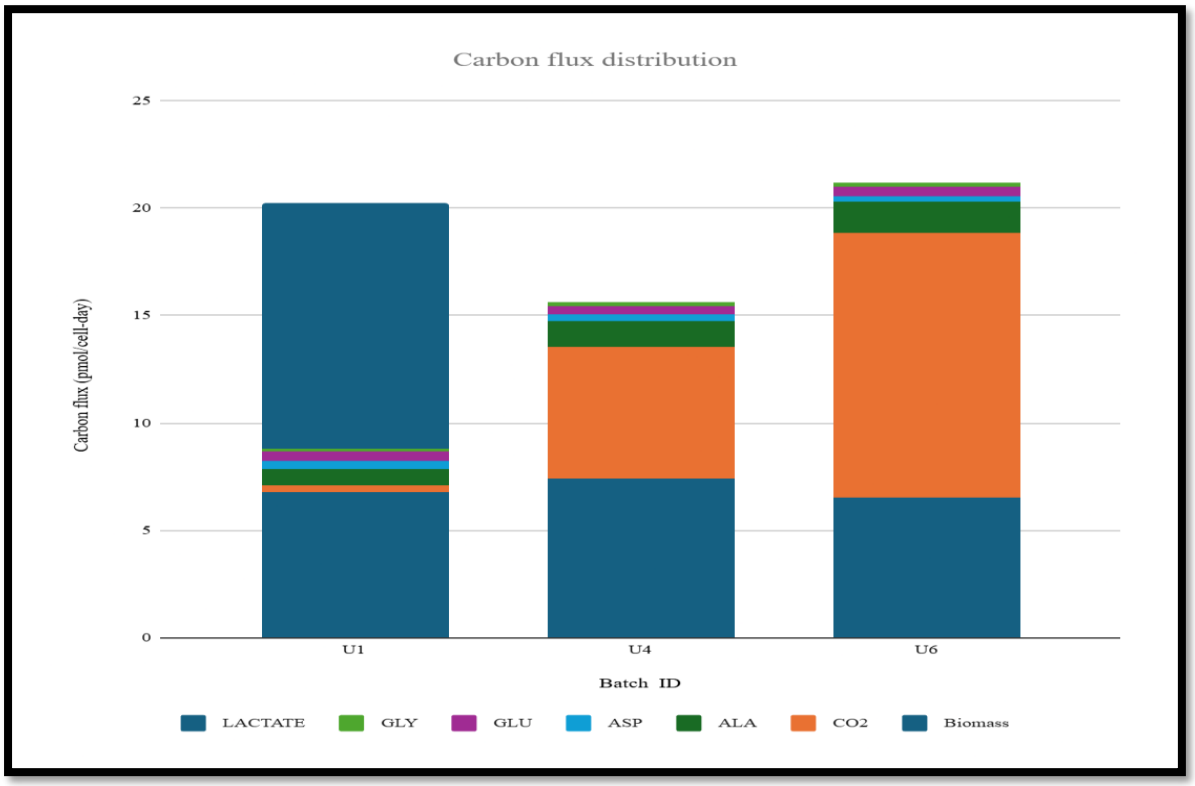

Figure 2: Carbon Flux Distribution during the Exponential Phase

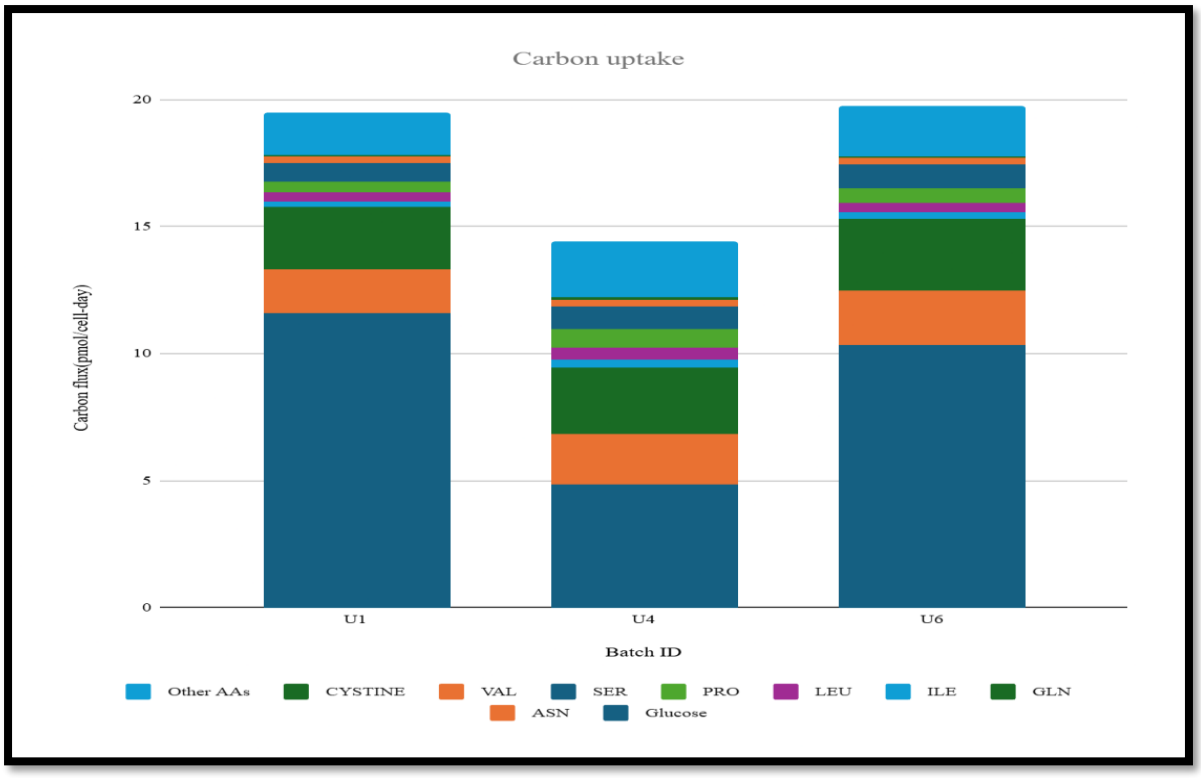

Figure 3: Carbon Uptake during the Exponential Phase

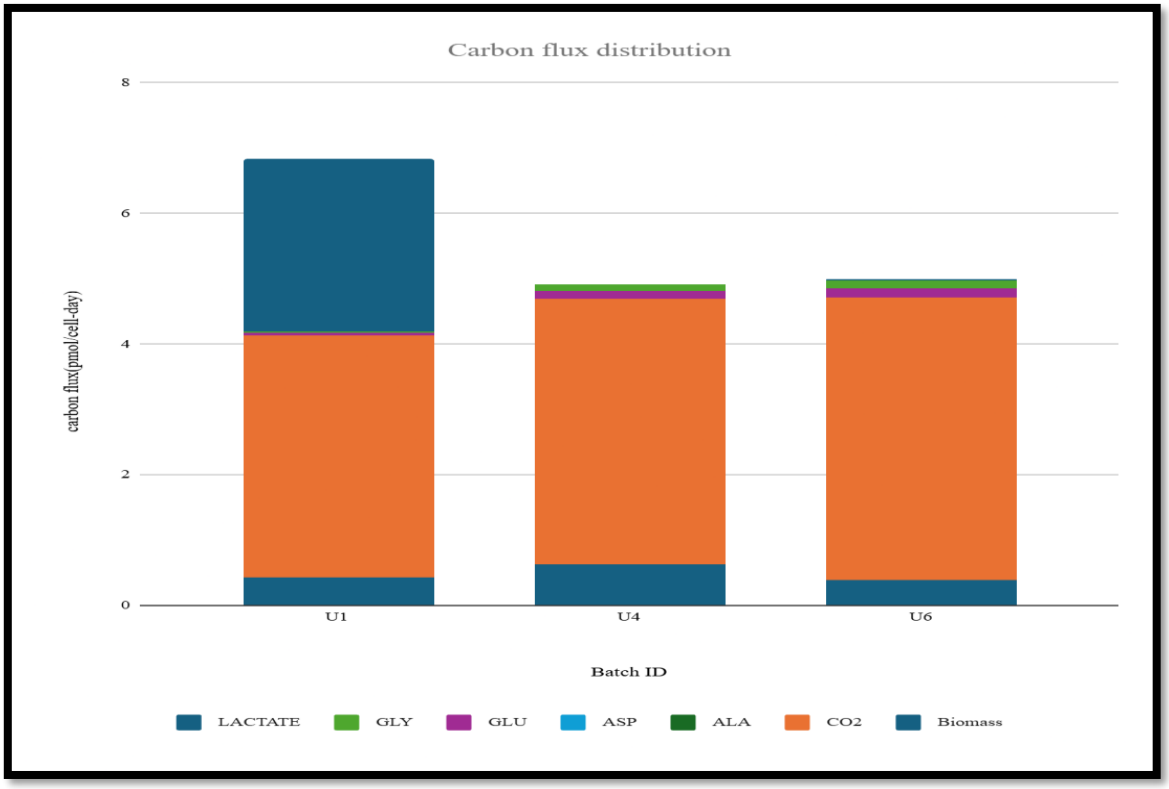

Figure 4: Carbon Flux Distribution during the Stationary Phase

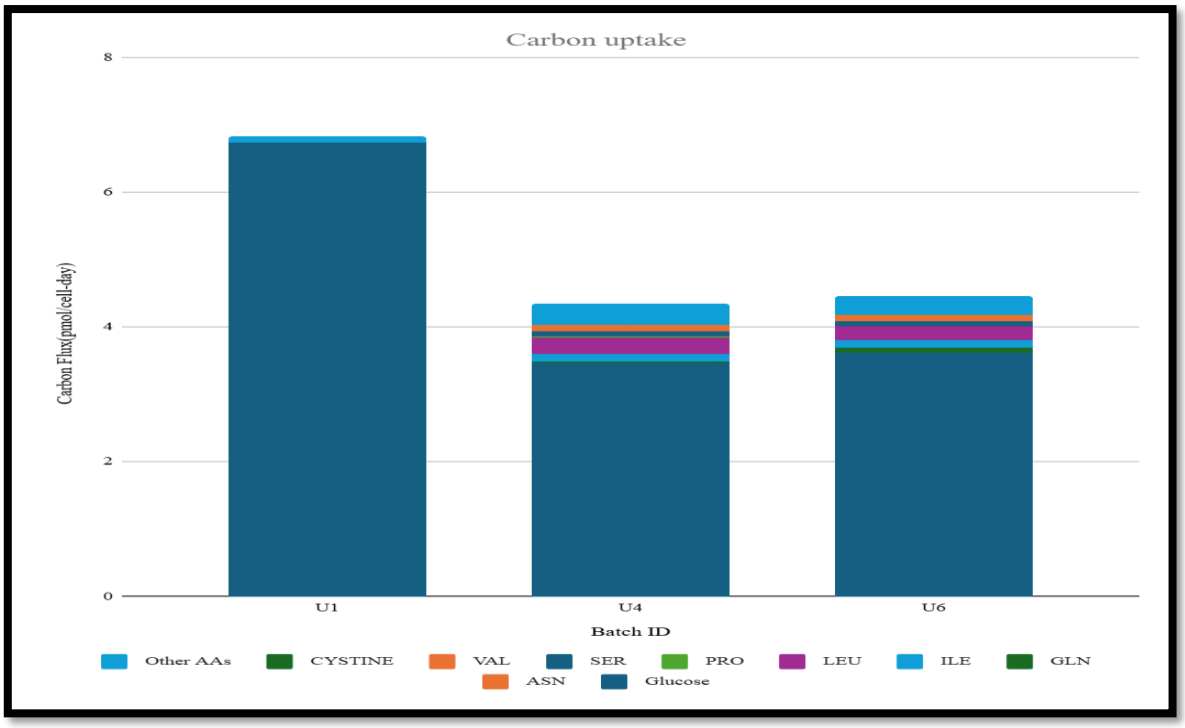

Figure 5: Carbon Uptake in the Stationary Phase

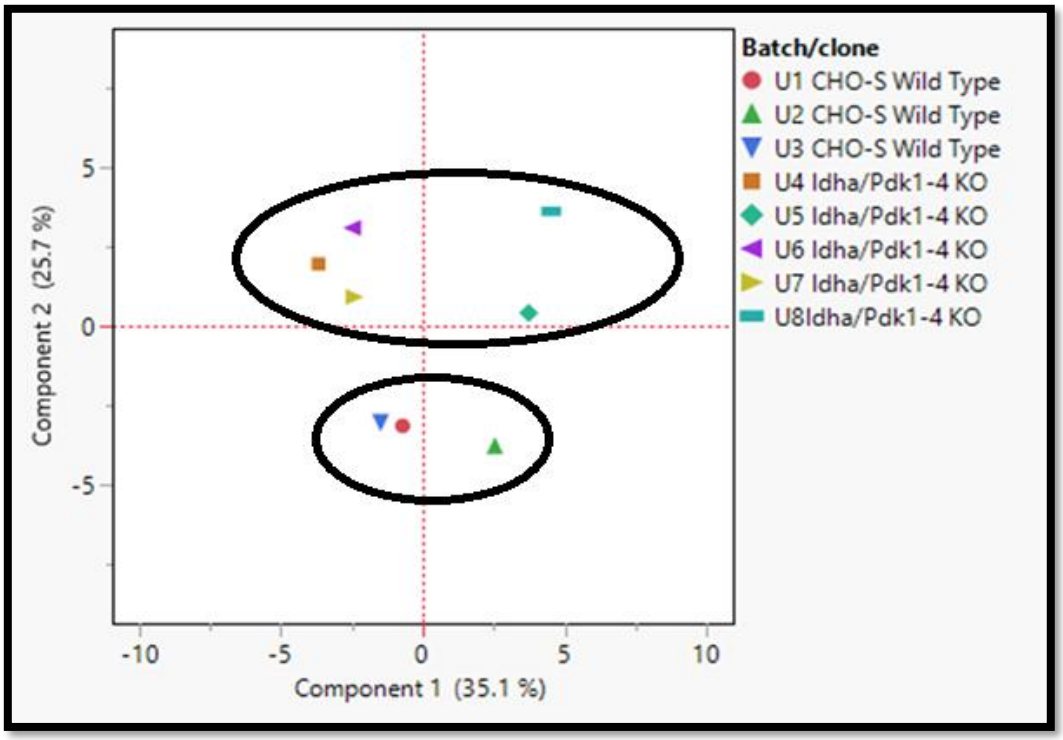

Figure 6: PCA for Exponential Phase

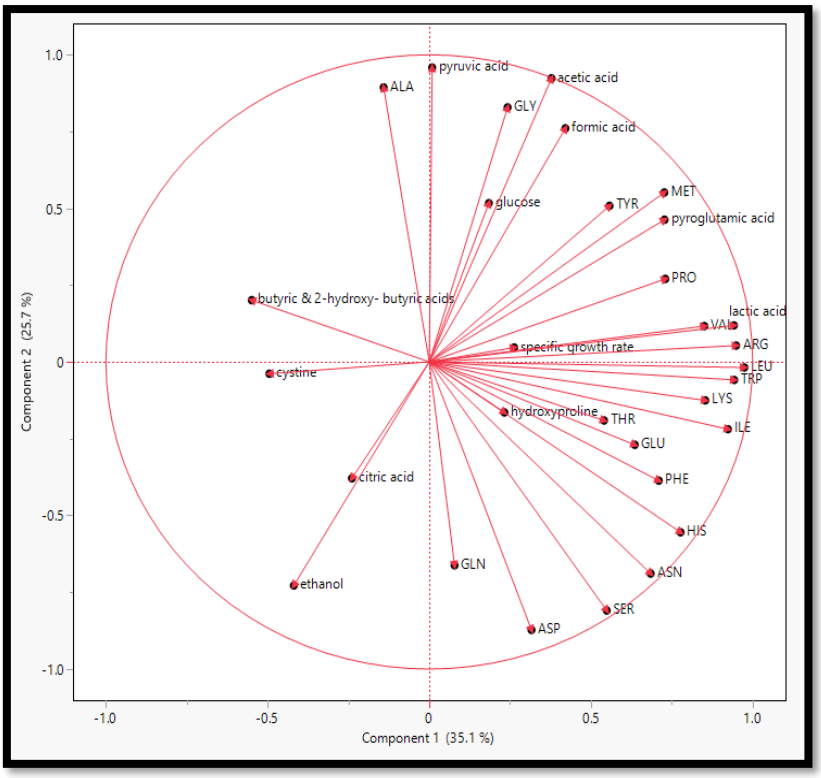

Figure 7: Loading plot (Exponential Phase PCA)

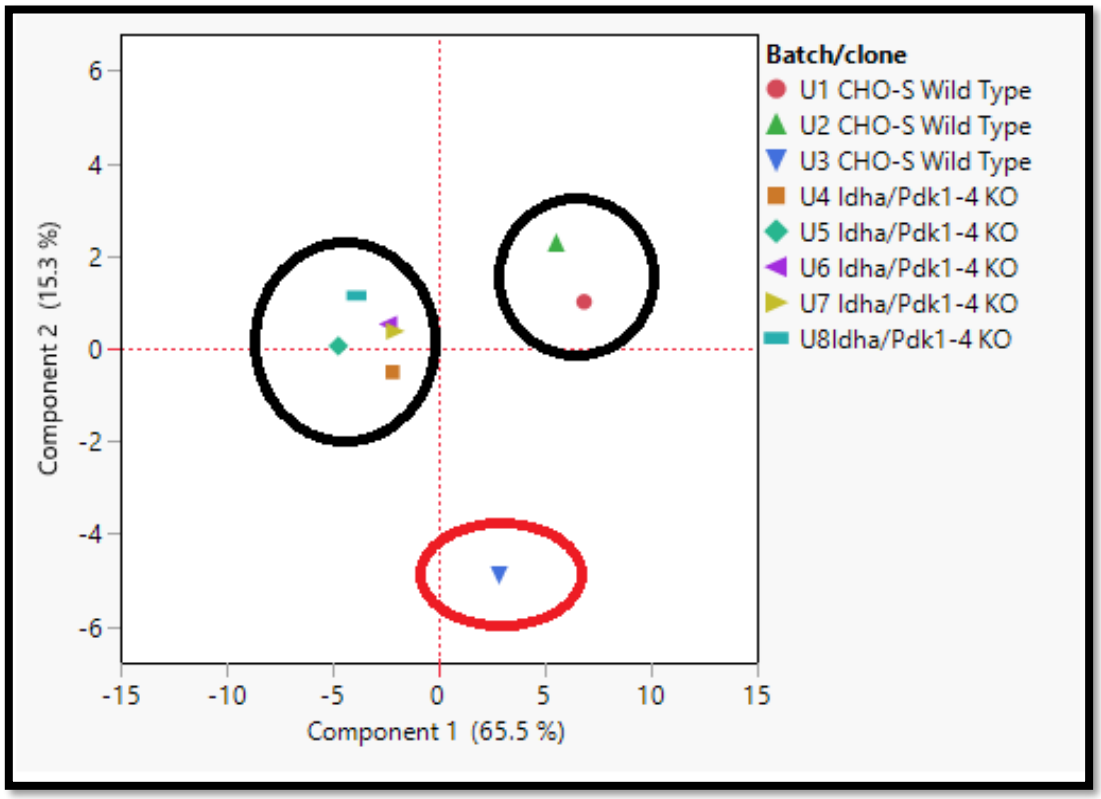

Figure 8: PCA for Stationary Phase

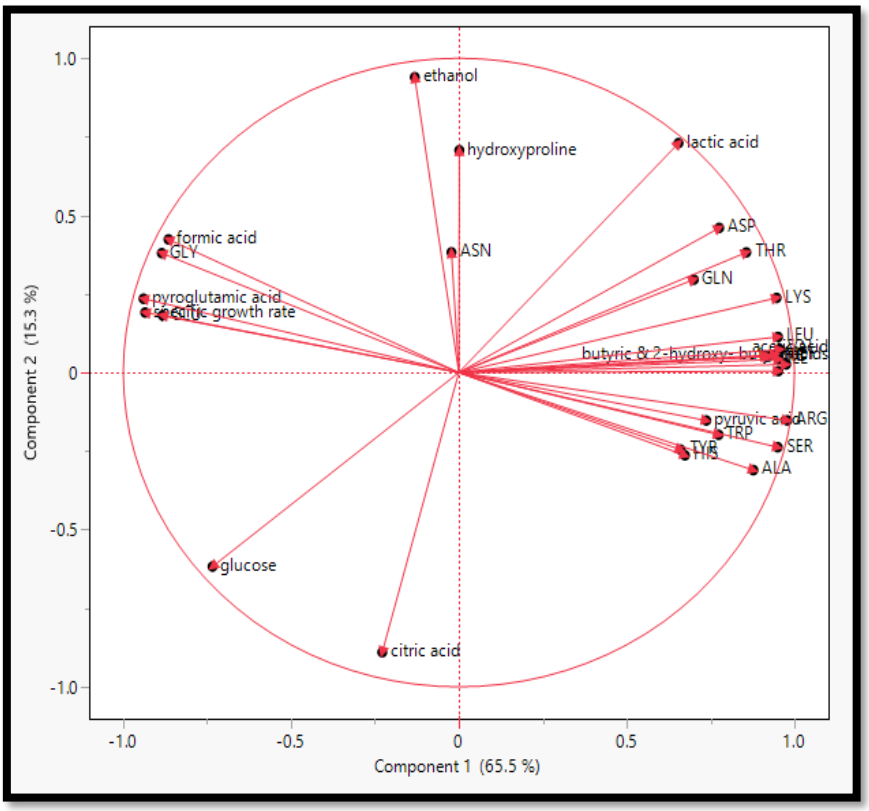

Figure 9: Loading plot (Stationary Phase PCA)

Batch Run	CHO-S Cell Line	Phase of cell growth	Specific Growth Rate (calculated using FBA, h^{-1})	Specific Growth Rate (experimental, h^{-1})	Calculated Value/Experimental Value
U1	WT	Exponential	0.033255361	0.03025	1.099350784
U1	WT	Stationary	0.002209223	0.00353	0.625842226
U4	LDHa/PDK-1 KO	Exponential	0.018036785	0.03177	0.567730097
U4	LDHa/PDK-1 KO	Stationary	0.002209223	0.00187	1.181402705
U6	LDHa/PDK-2 KO	Exponential	0.018036785	0.02819	0.639829202
U6	LDHa/PDK-2 KO	Stationary	0.002209223	0.00266	0.830534984

Table 1: Comparison of calculated and experimental specific growth rates

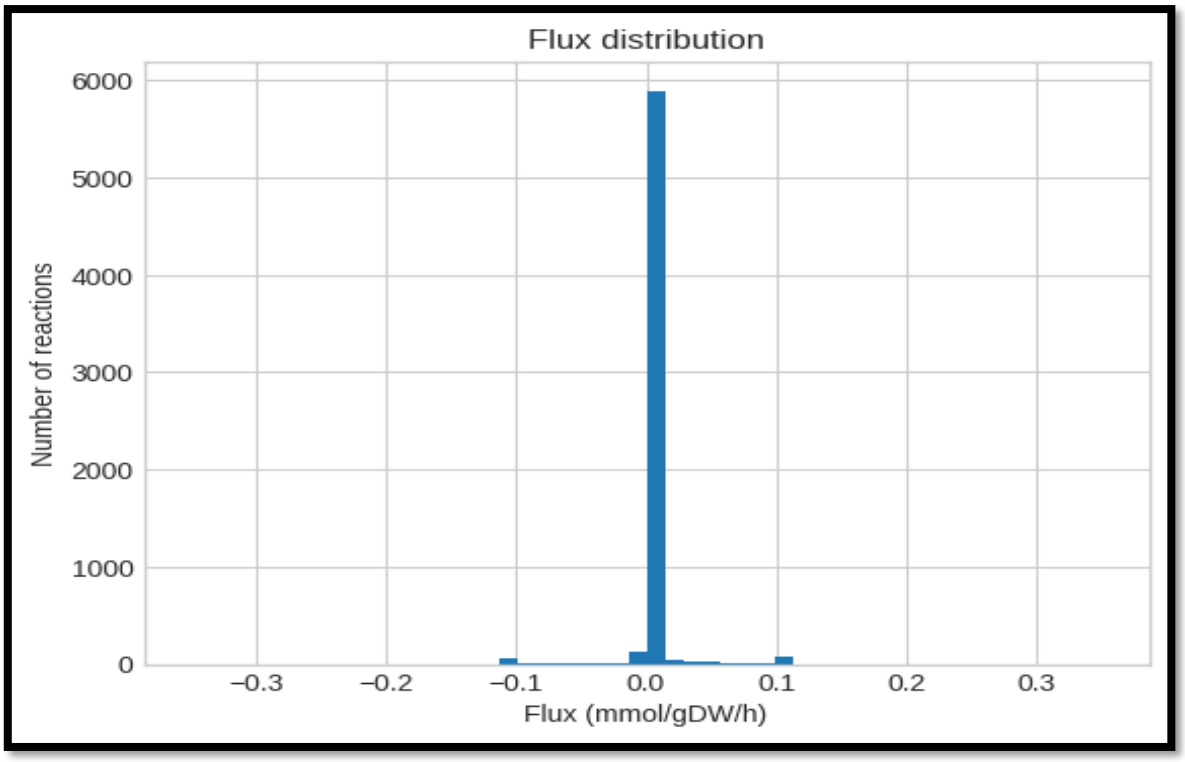

Figure 10: (Exponential Phase of the WT CHO-S Cell Line) Flux Distribution

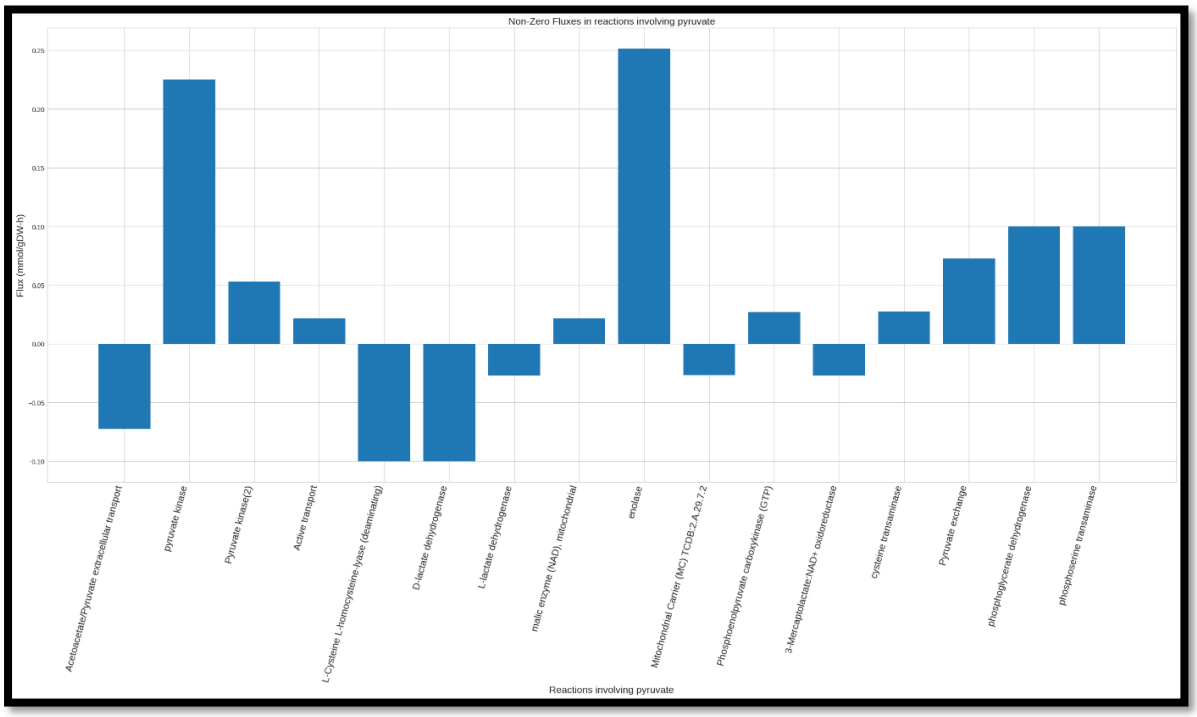

Figure 11: (Exponential Phase of the WT CHO-S Cell Line) Fluxes through reactions involving Pyruvate

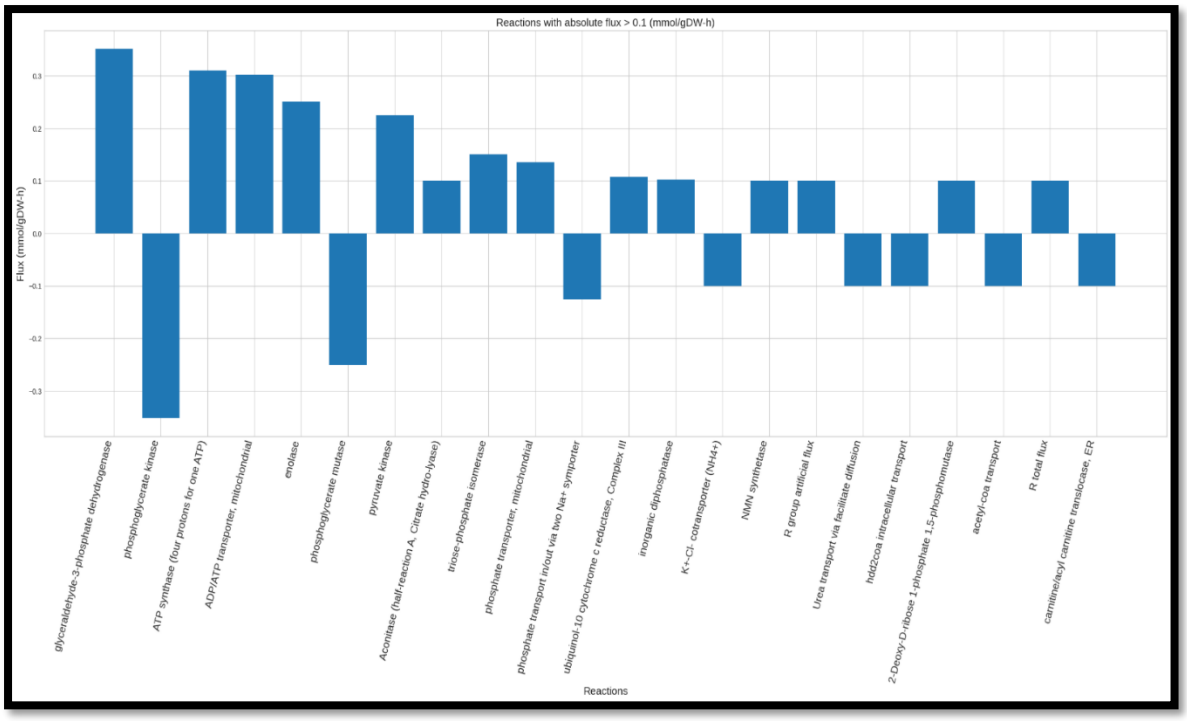

Figure 12: (Exponential Phase of the WT CHO-S Cell Line) Reactions with flux > 0.1 $\frac{mmol}{gDW-h}$:

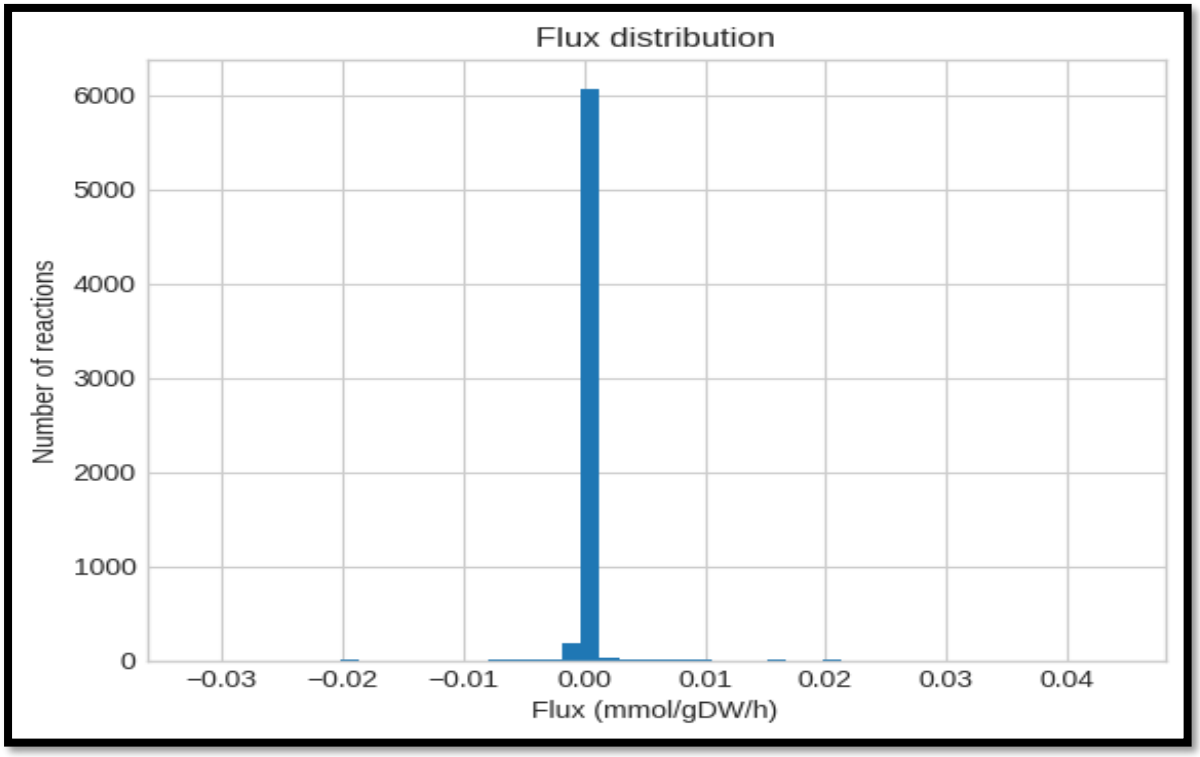

Figure 13: (Stationary Phase of the WT CHO-S cell line) Flux Distribution

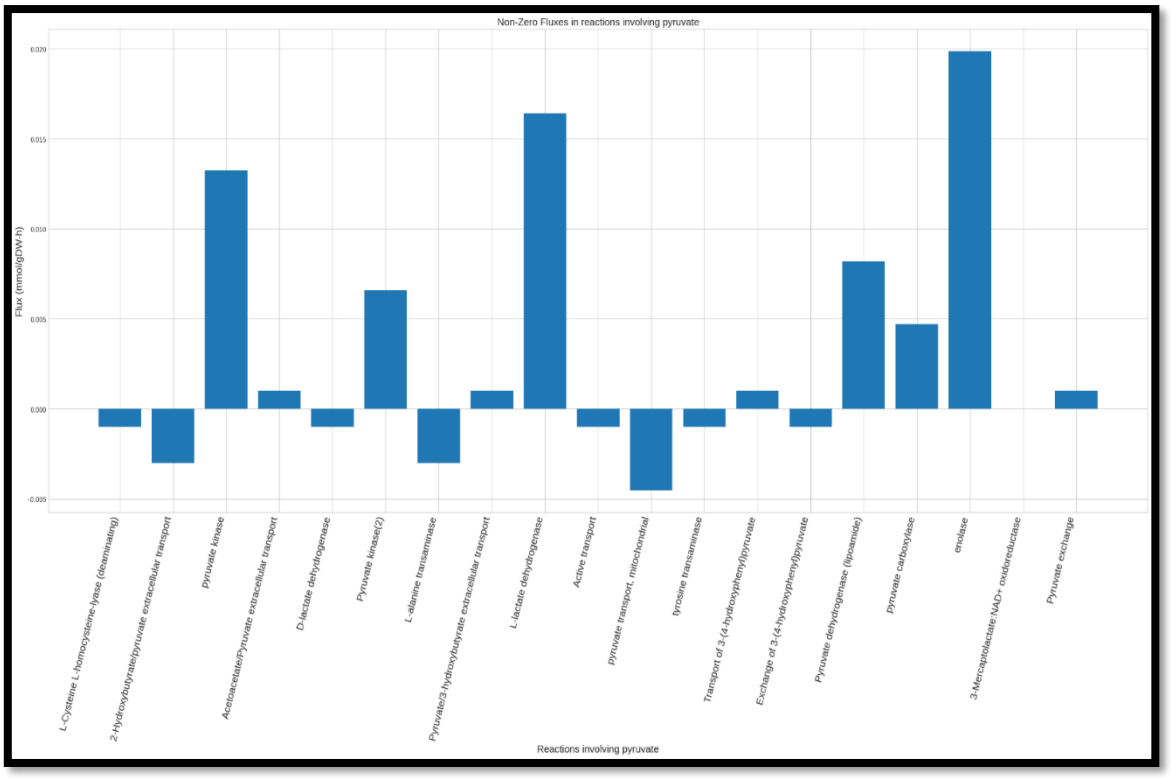

Figure 14: (Stationary Phase of the WT CHO-S cell line) Fluxes through reactions involving Pyruvate

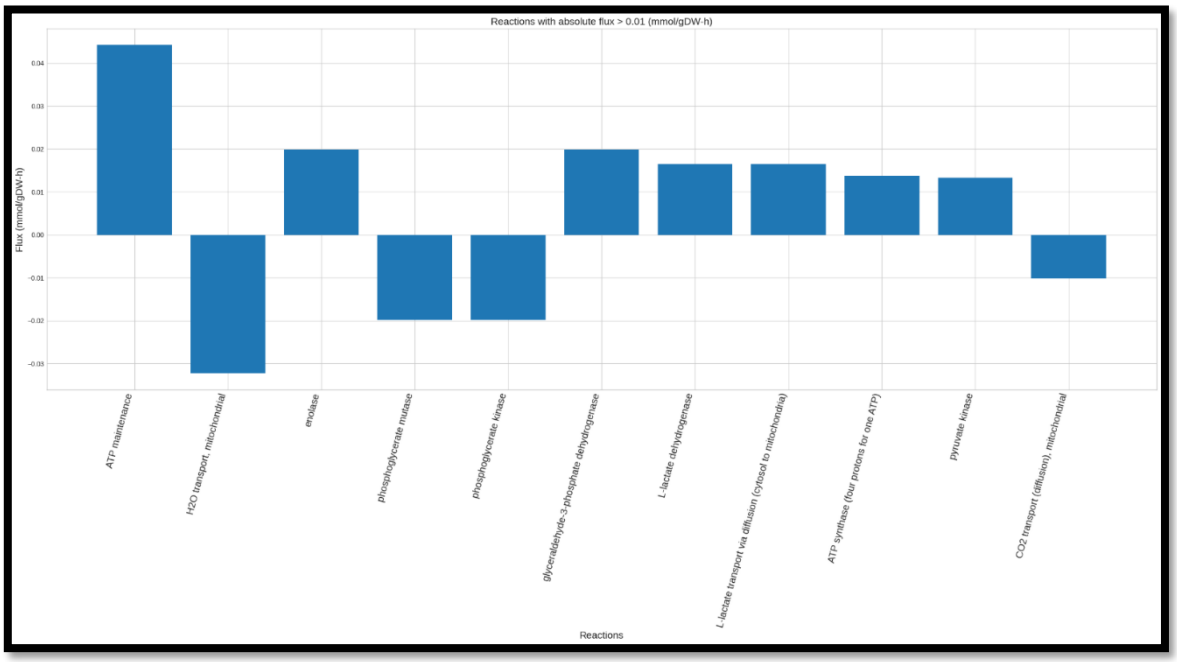

Figure 15: (Stationary Phase of the WT CHO-S cell line) Reactions with flux > 0.01 $\frac{mmol}{gDW-h}$:

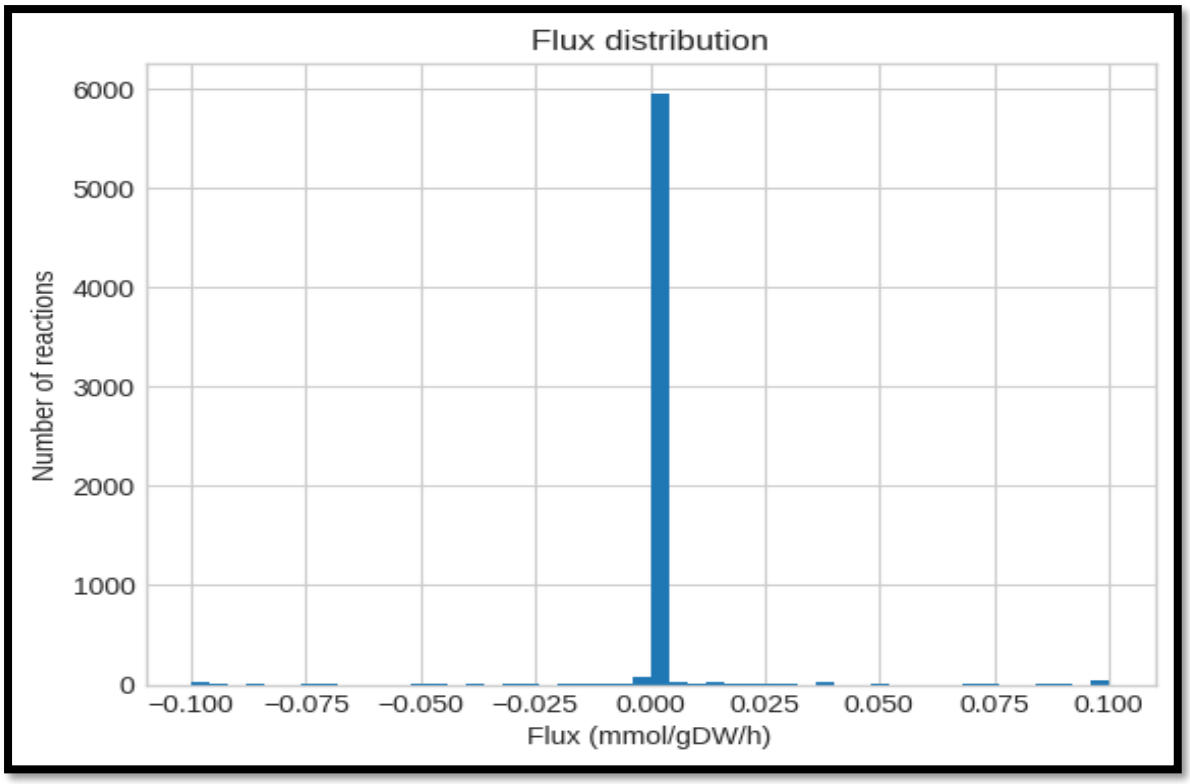

Figure 16: (Exponential Phase of the LDHa/PDK-1 KO CHO-S cell line) Flux Distribution

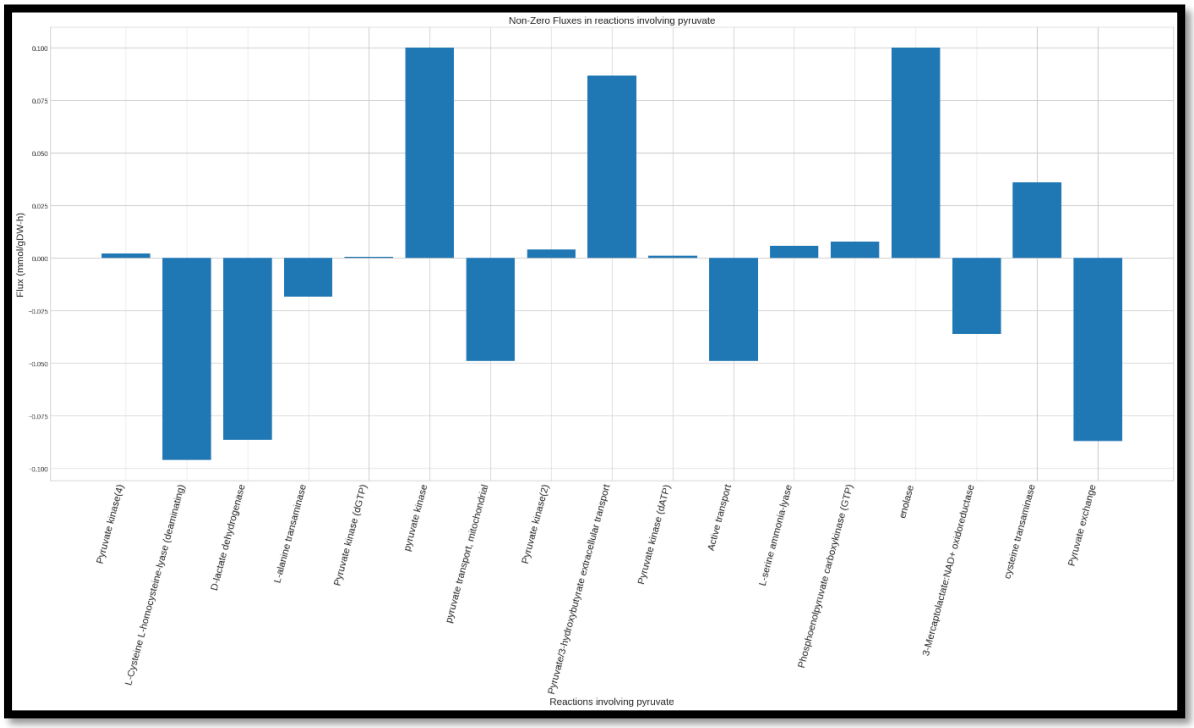

Figure 17: (Exponential Phase of the LDHa/PDK-1 KO CHO-S cell line) Fluxes through reactions involving Pyruvate

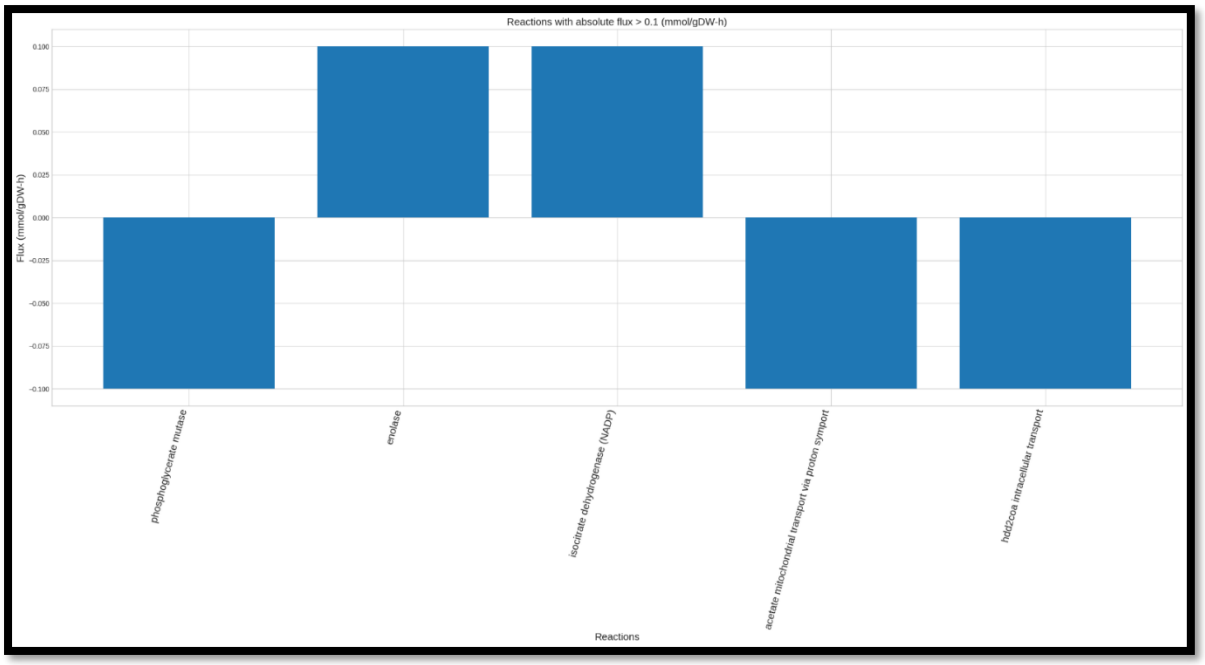

Figure 18: (Exponential Phase of the LDHa/PDK-1 KO CHO-S cell line)
Reactions with flux > 0.01 $\frac{mmol}{gDW-h}$:

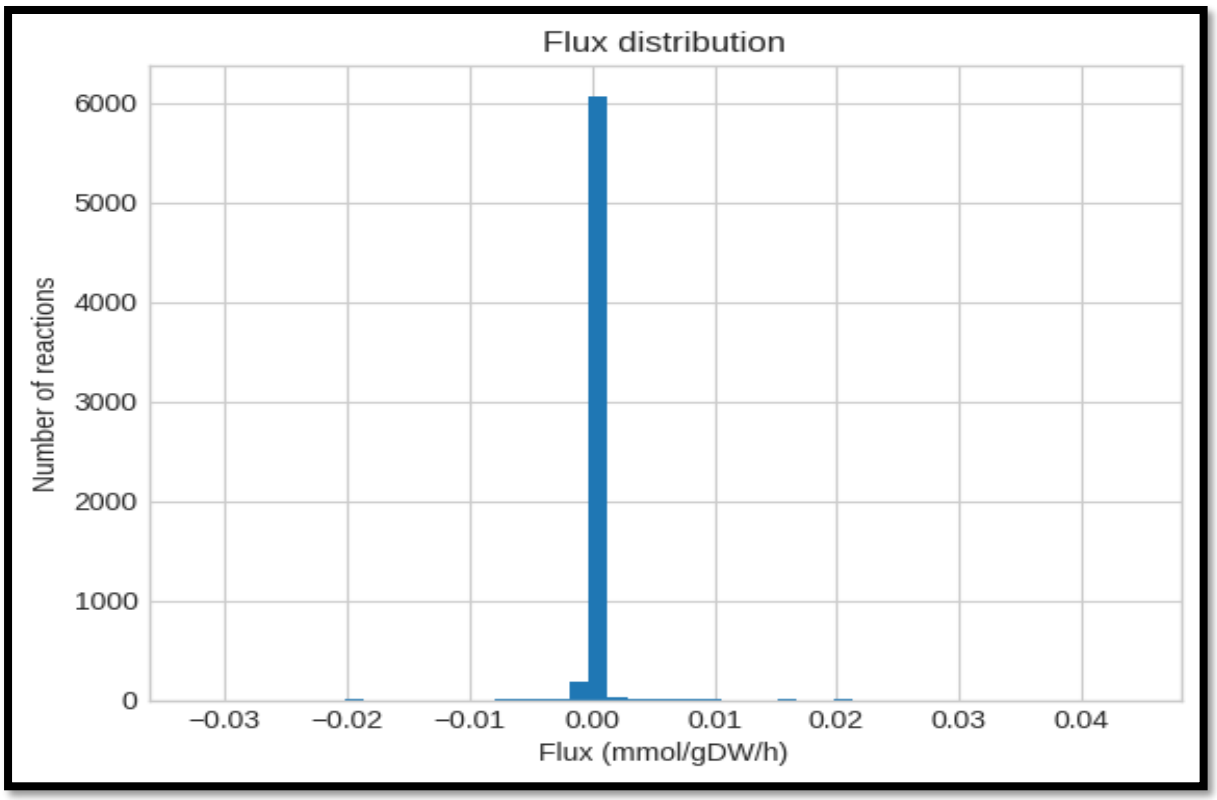

Figure 19: (Stationary Phase of the LDHa/PDK-1 KO CHO-S cell line) Flux Distribution

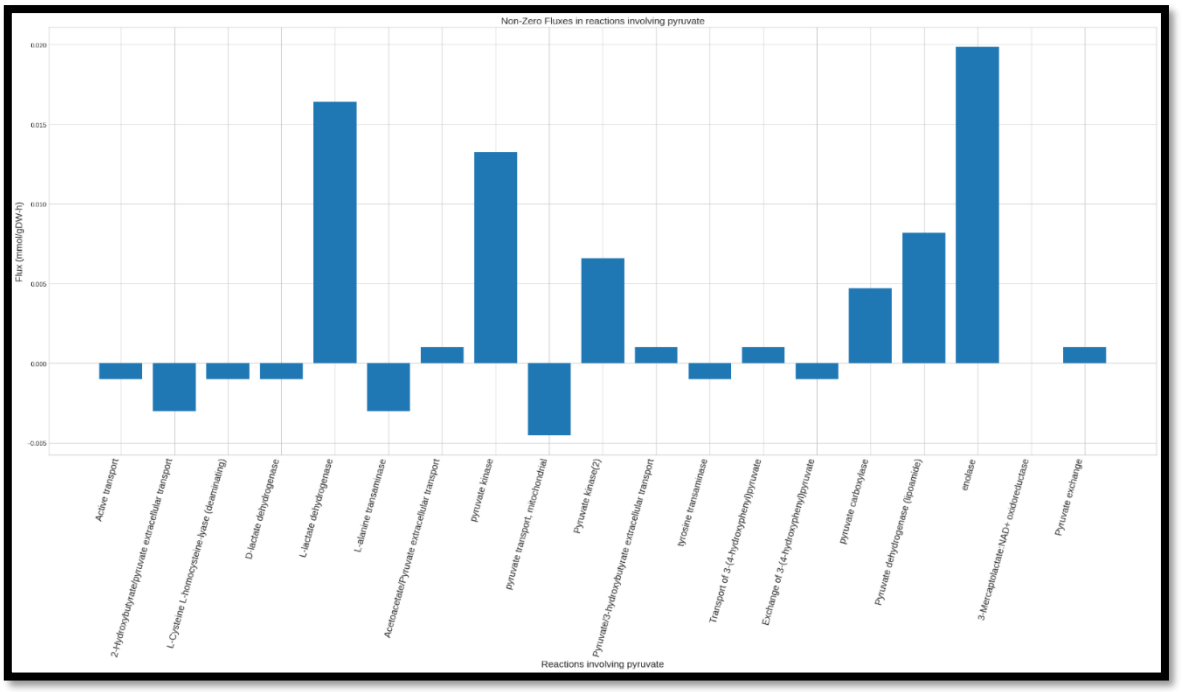

Figure 20: (Stationary Phase of the LDHa/PDK-1 KO CHO-S cell line)
Fluxes through reactions involving Pyruvate

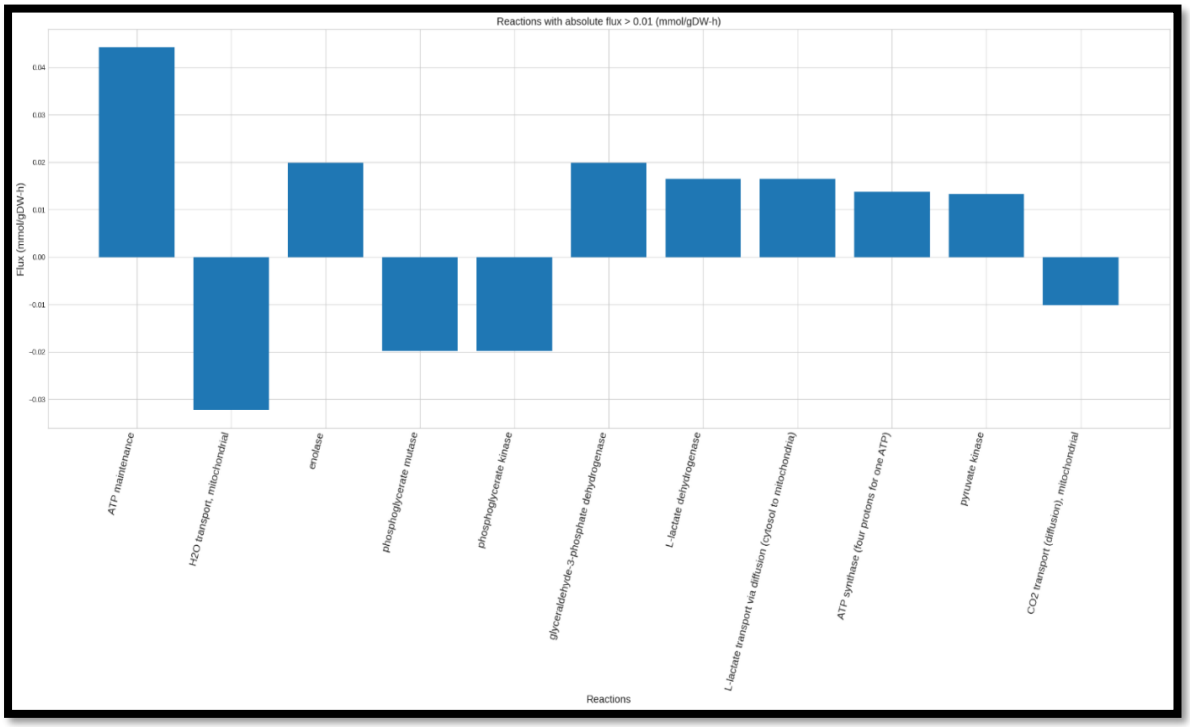

Figure 21: (Stationary Phase of the LDHa/PDK-1 KO CHO-S cell line)
Reactions with flux > 0.01 mmol/(gDW-h)

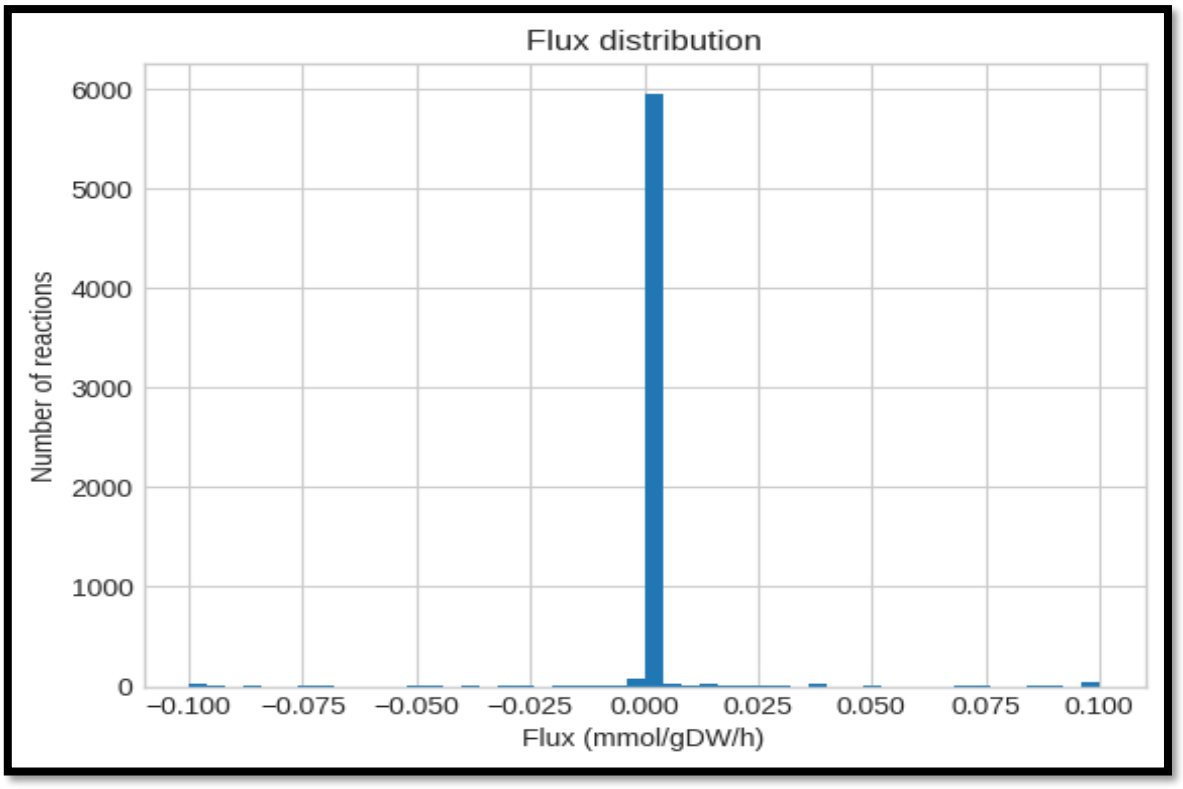

Figure 22: (Exponential Phase of the LDHa/PDK-2 KO CHO-S cell line) Flux Distribution

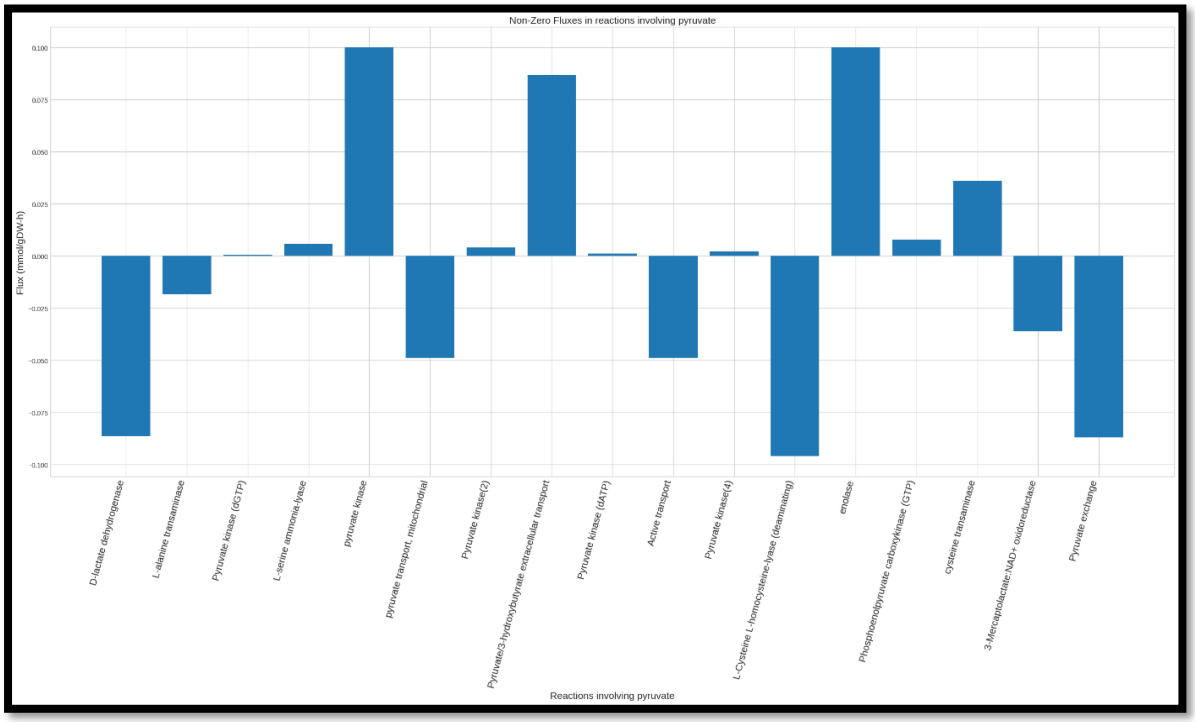

Figure 23: (Exponential Phase of the LDHa/PDK-2 KO CHO-S cell line)

Flux through reactions involving Pyruvate

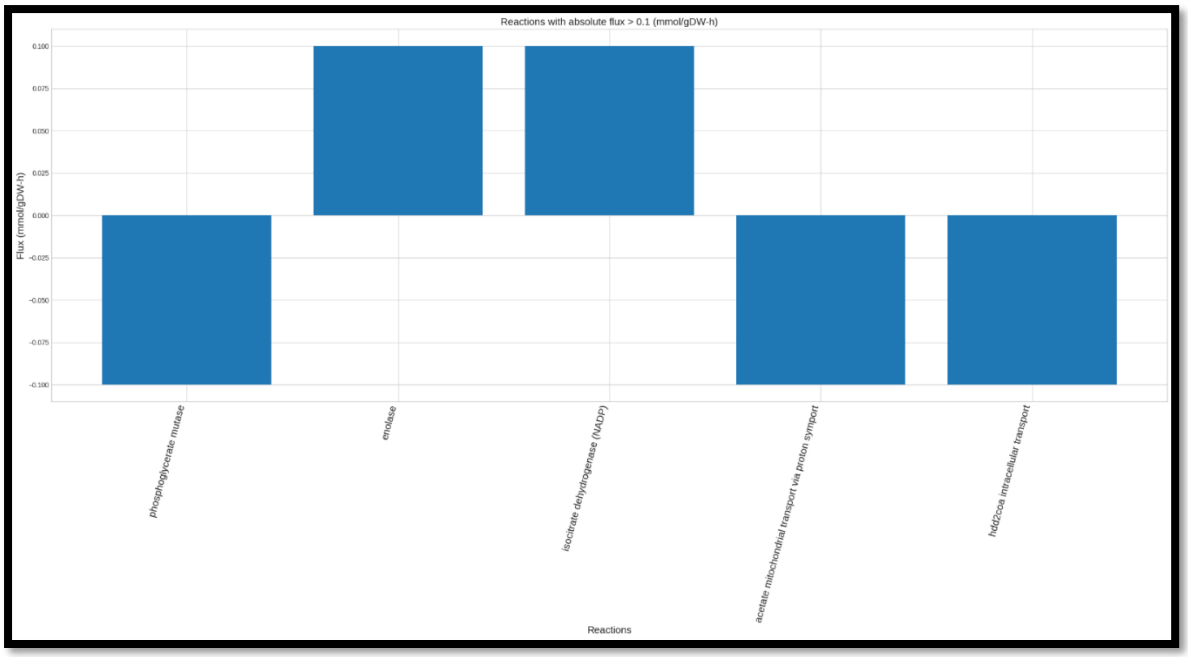

Figure 24: (Exponential Phase of the LDHa/PDK-2 KO CHO-S cell line)

Reactions with flux > 0.1 $\frac{mmol}{gDW-h}$

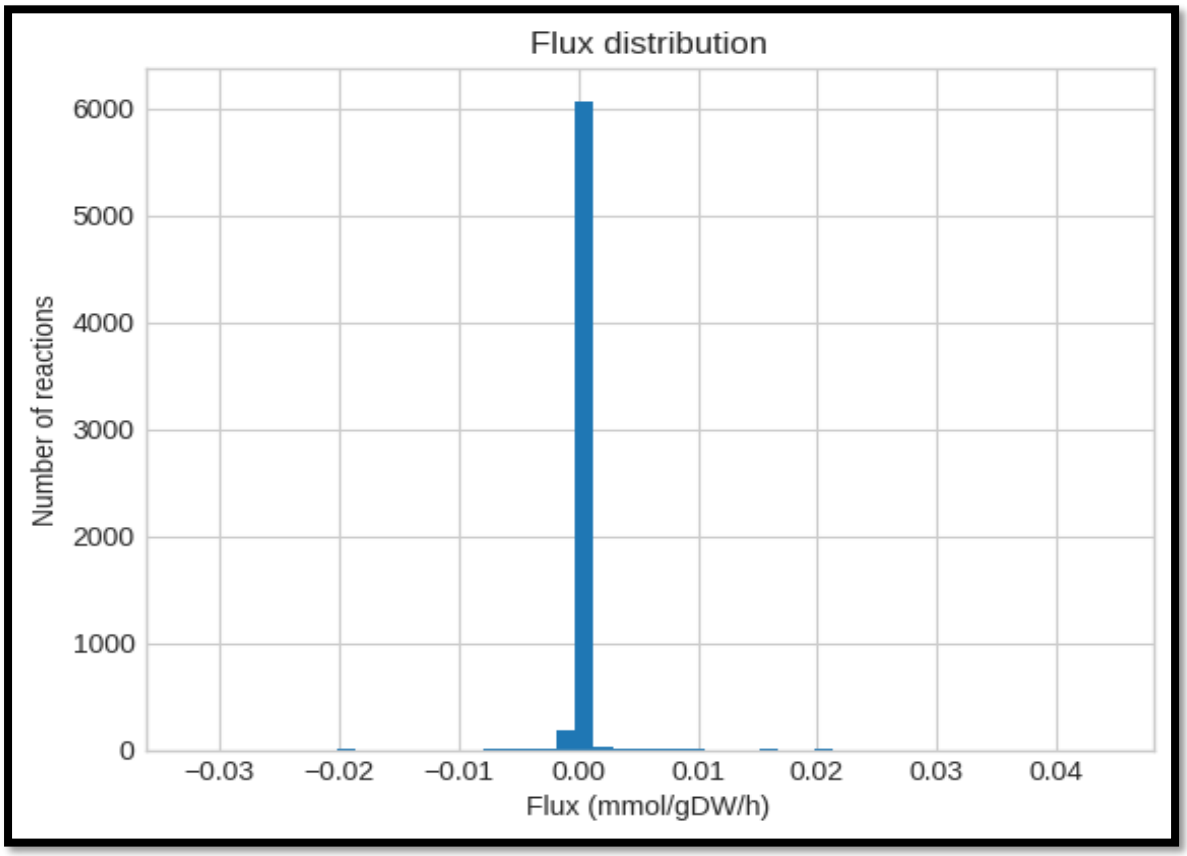

Figure 25: (Stationary Phase of the LDHa/PDK-2 KO CHO-S cell line) Flux Distribution

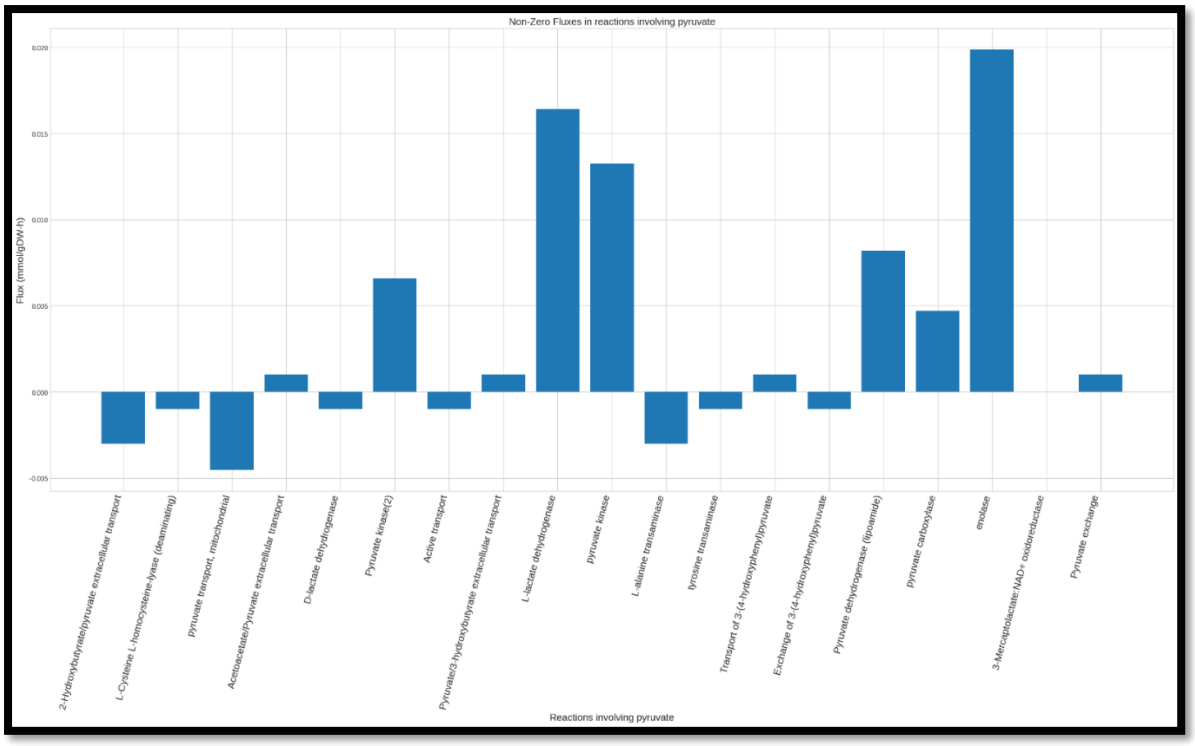

Figure 26: (Stationary Phase of the LDHa/PDK-2 KO CHO-S cell line)

Flux through reactions involving Pyruvate

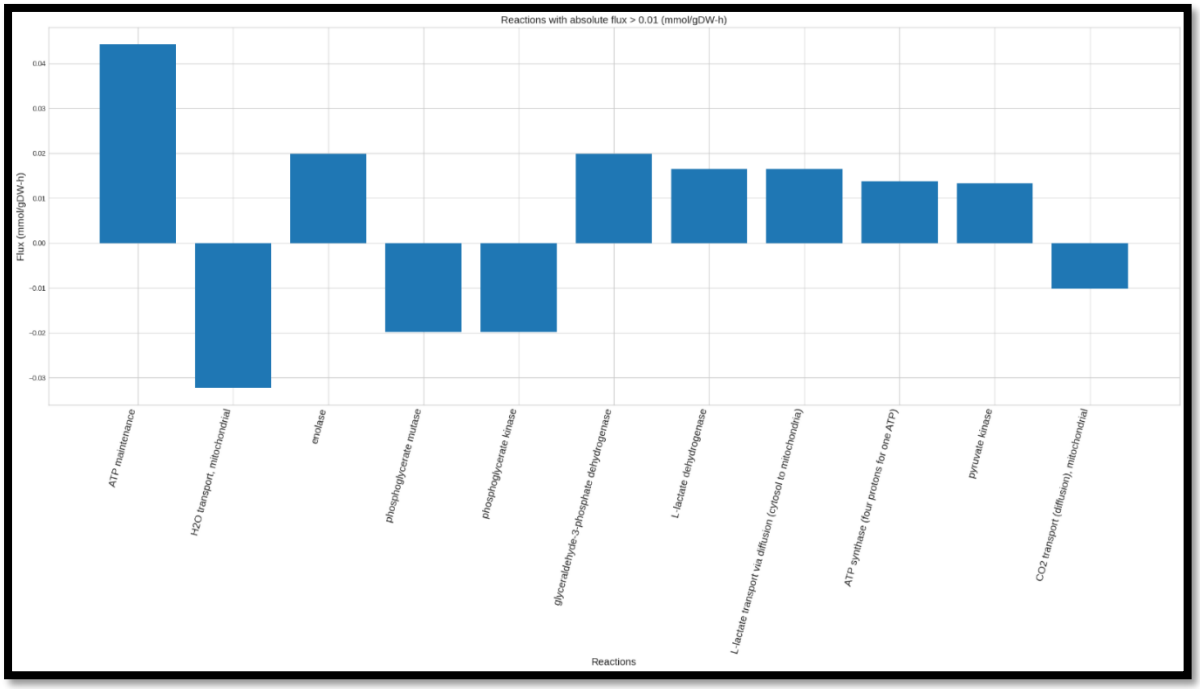

Figure 27: (Stationary Phase of the LDHa/PDK-2 KO CHO-S cell line)

Reactions with flux > 0.01 mmol/(gDW-h):

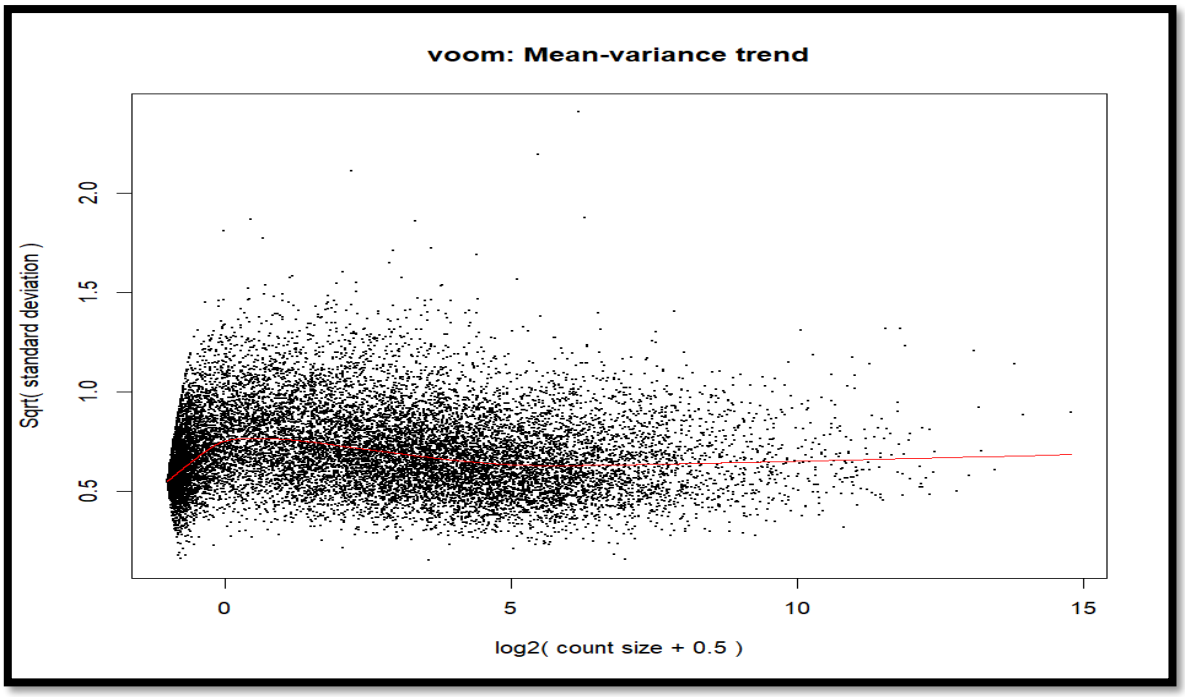

Figure 28: Voom fitting on Exponential Phase data

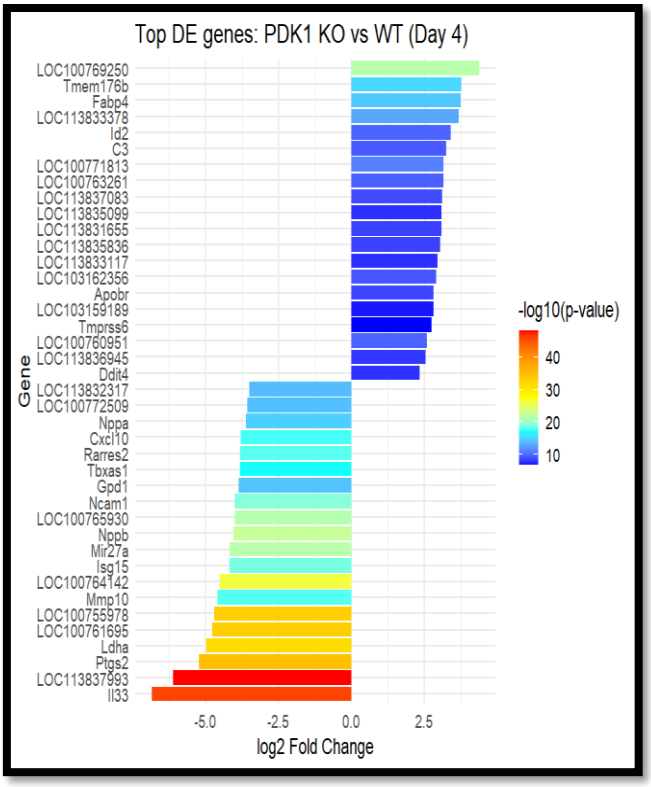

Figure 29: Differentially Expressed Genes in LDHa/PDK1 KO vs WT (Exponential Phase)

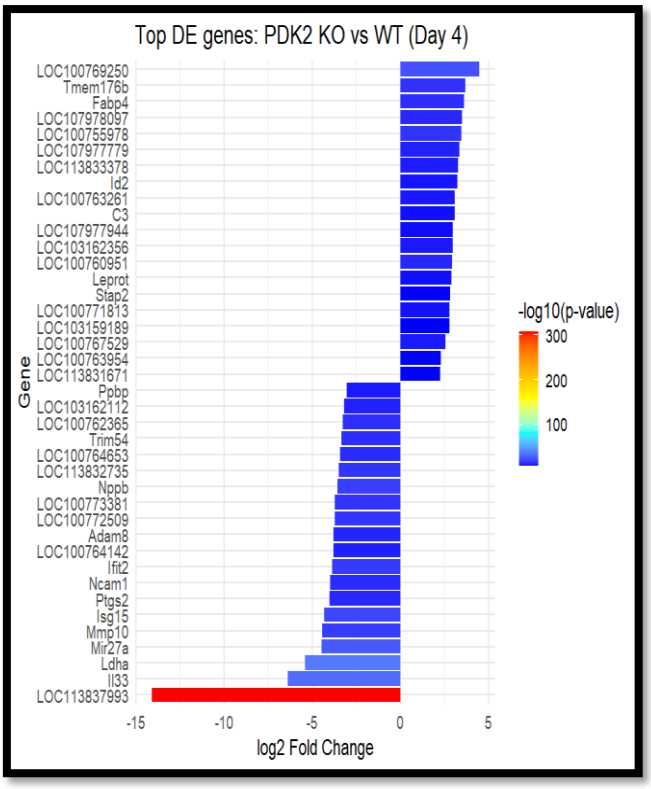

Figure 30: Differentially Expressed Genes in LDHa/PDK2 KO vs WT (Exponential Phase)

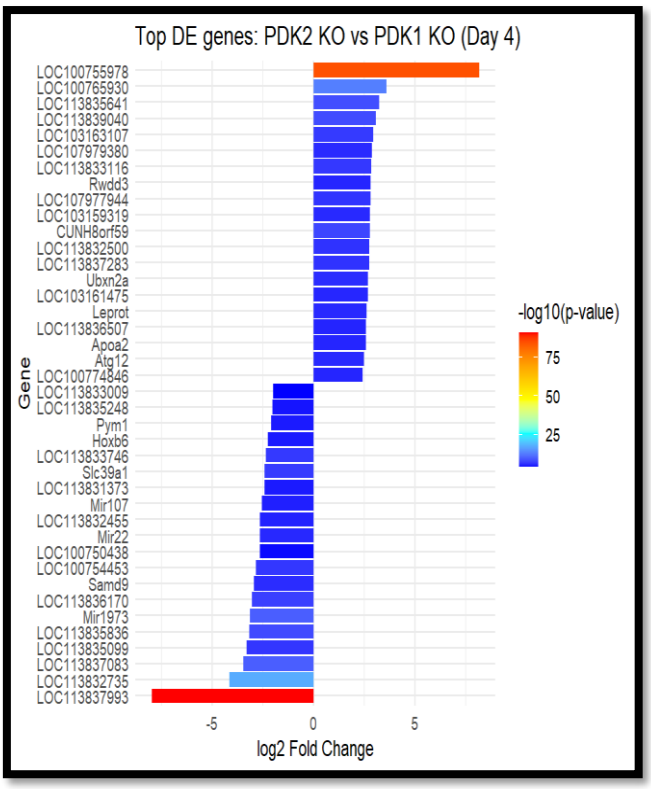

Figure 31: Differentially Expressed Genes in LDHa/PDK2 KO vs LDHa/PDK1 (Exponential Phase)

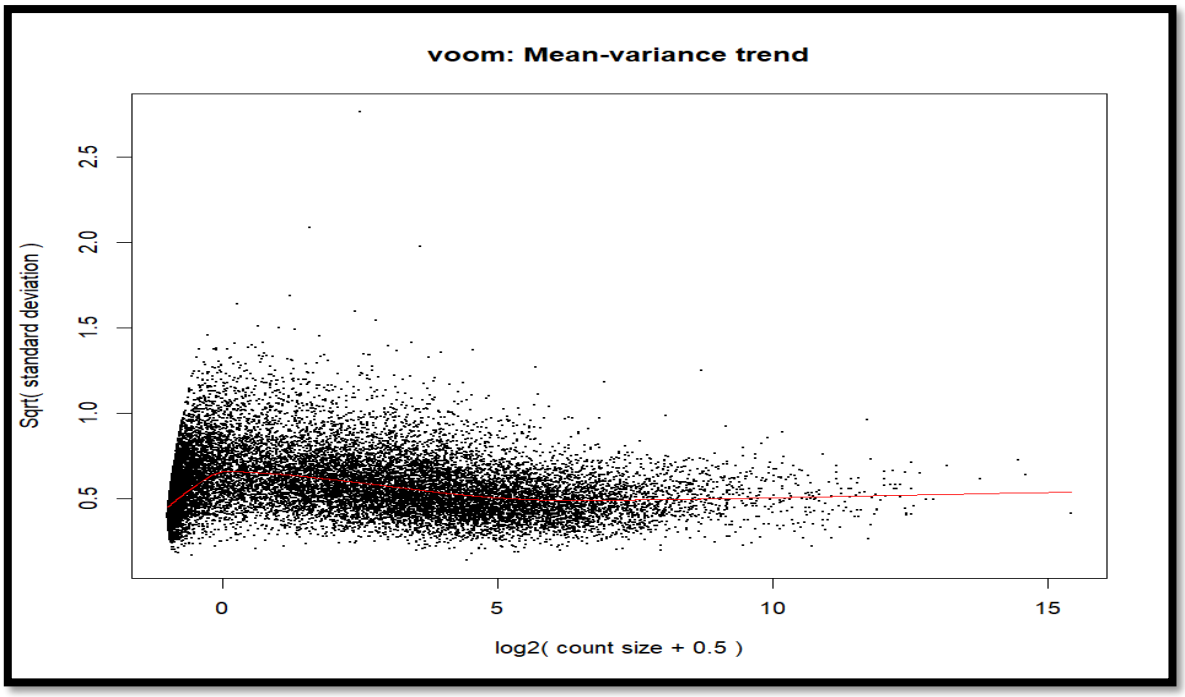

Figure 32: Voom fitting on Stationary Phase data

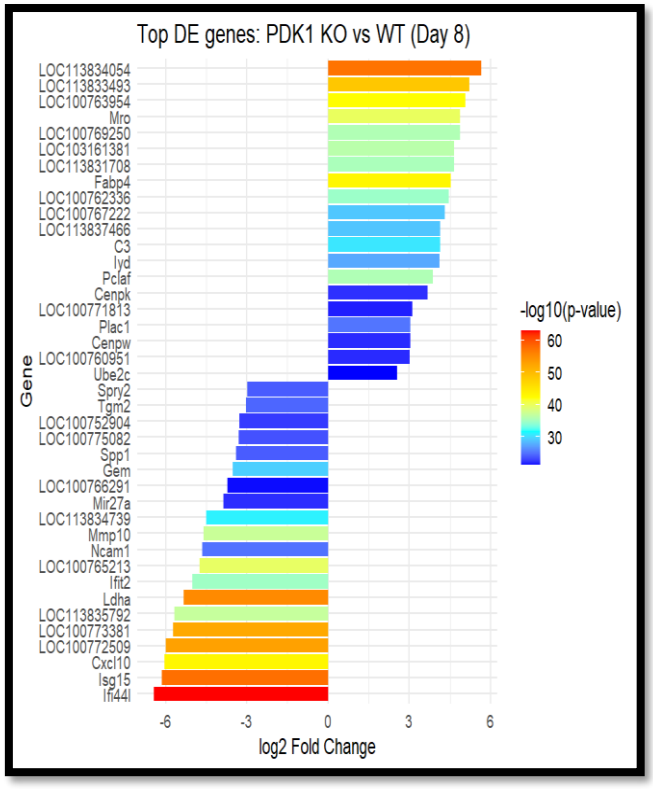

Figure 33: Differentially Expressed Genes in LDHa/PDK1 KO vs WT (Stationary Phase)

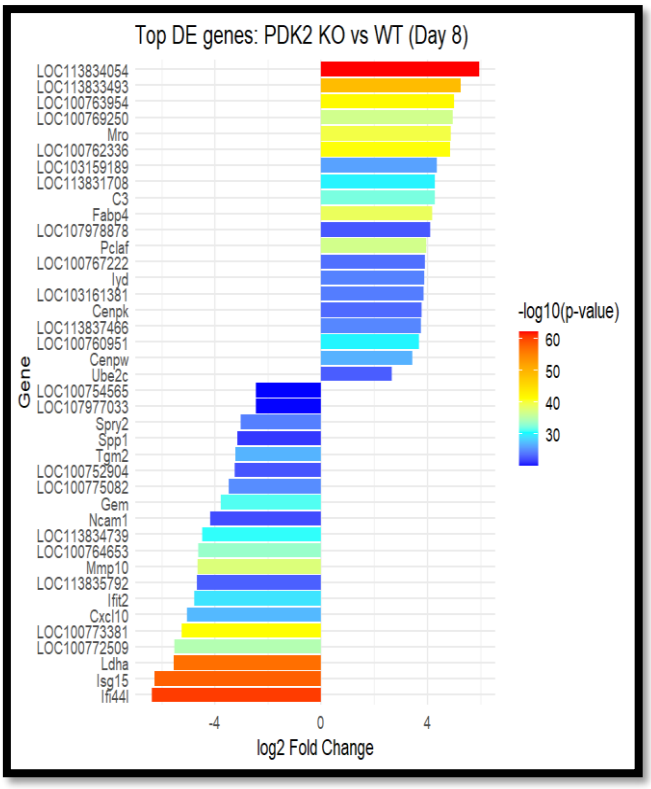

Figure 34: Differentially Expressed Genes in LDHa/PDK2 KO vs WT (Stationary Phase)

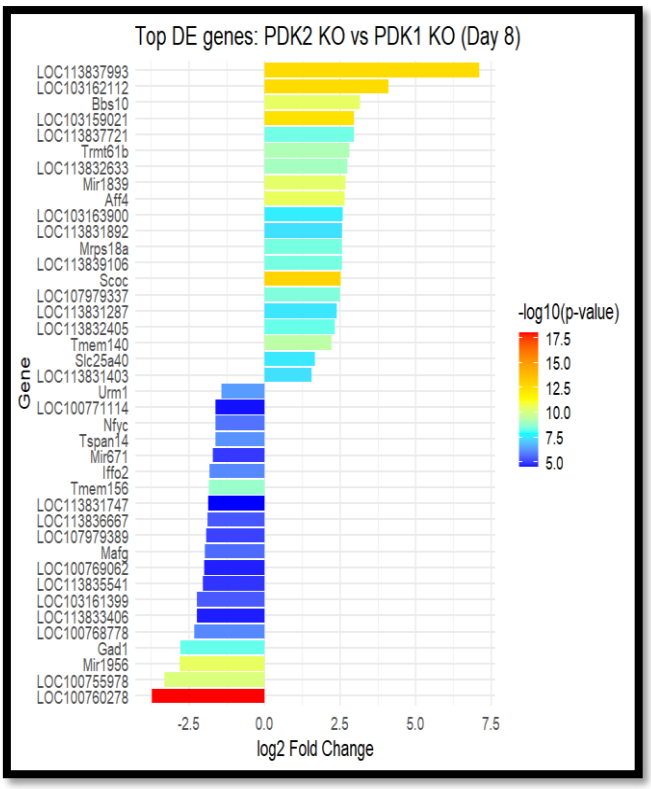

Figure 35: Differentially Expressed Genes in LDHa/PDK2 KO vs LDHa/PDK1 KO (Stationary Phase)

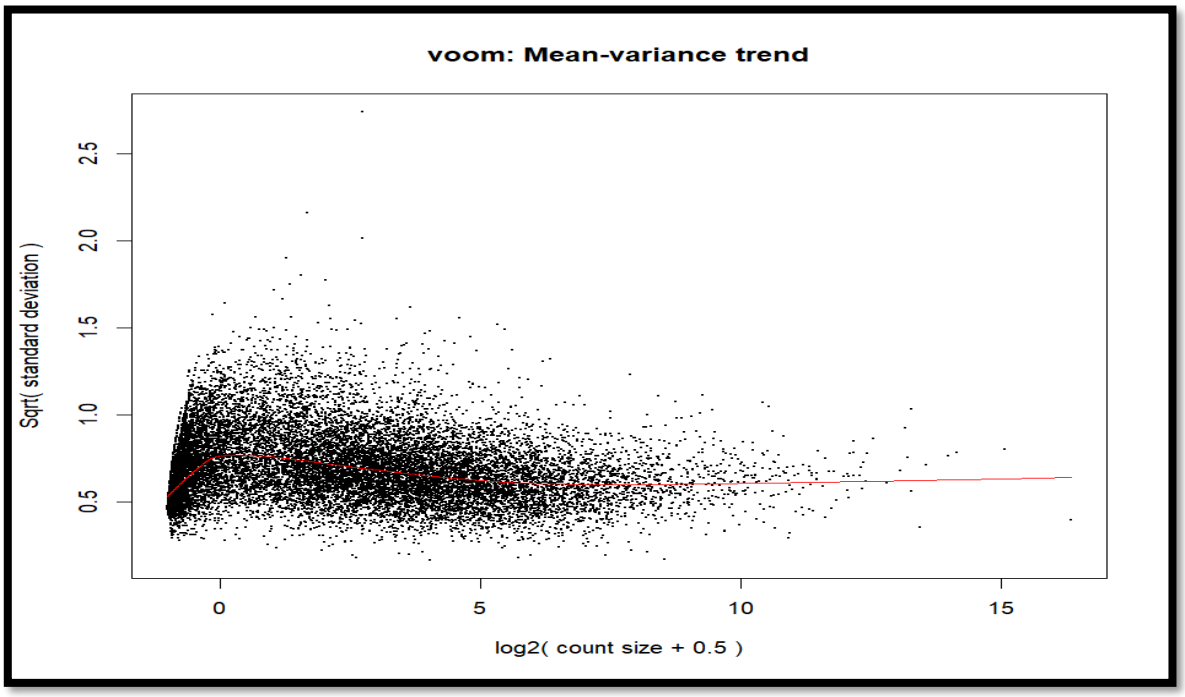

Figure 36: Voom fitting on Death Phase data

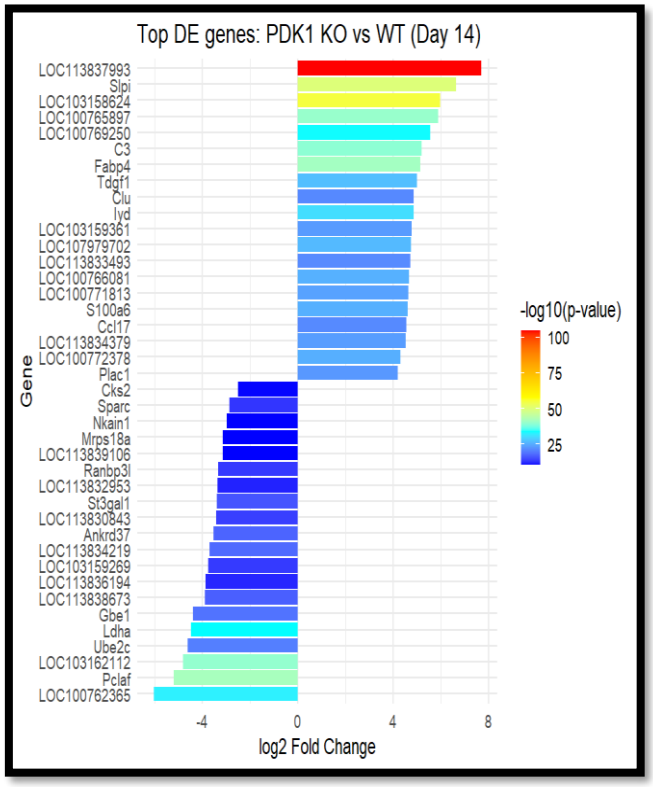

Figure 37: Differentially Expressed Genes in LDHa/PDK1 KO vs WT (Death Phase)

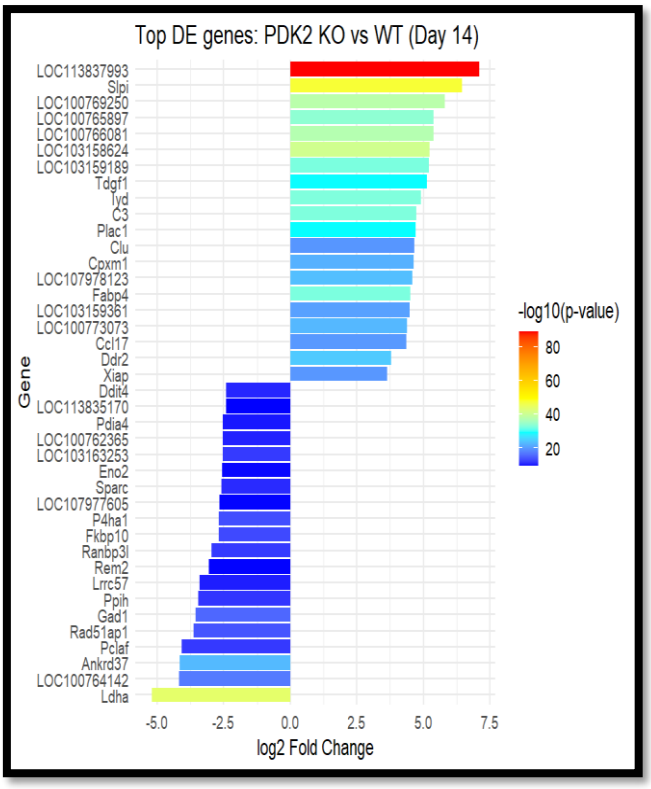

Figure 38: Differentially Expressed Genes in LDHa/PDK2 KO vs WT (Death Phase)

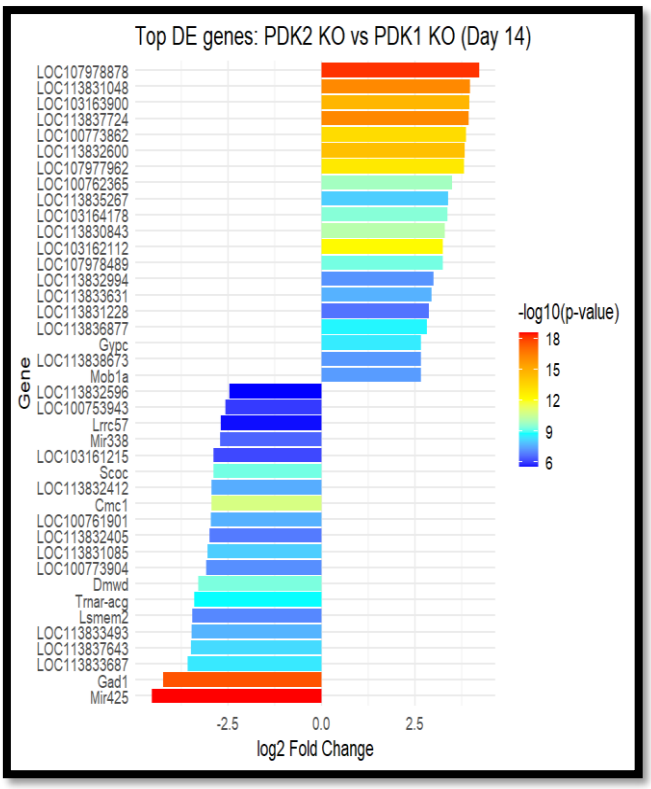

Figure 39: Differentially Expressed Genes in LDHa/PDK2 KO vs LDHa/PDK1 KO (Death Phase)

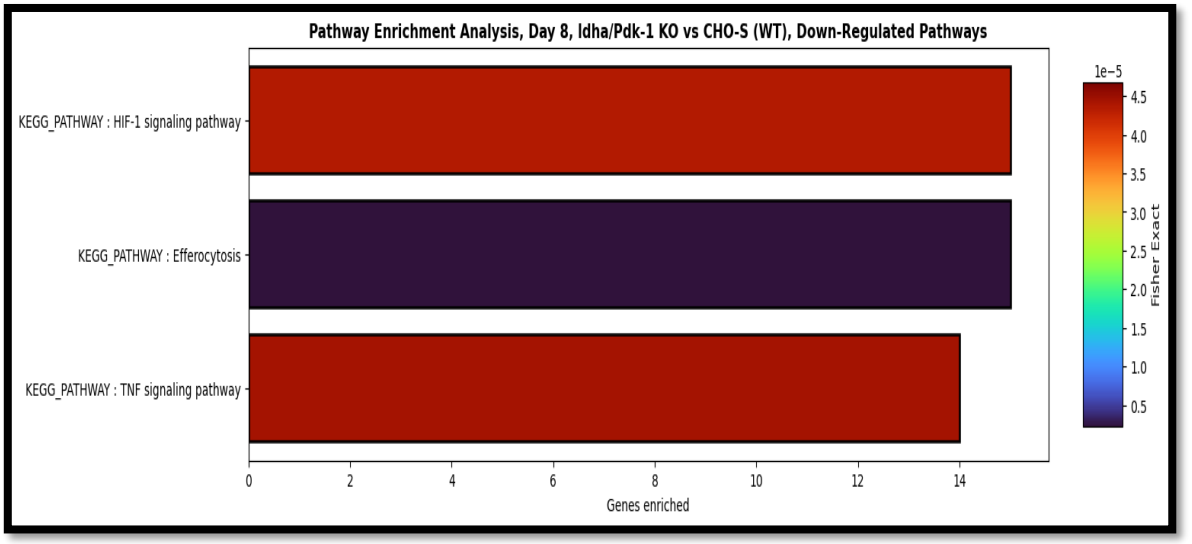

Figure 40: Stationary Phase Down-regulated pathways in LDHa/PDK-1 KO

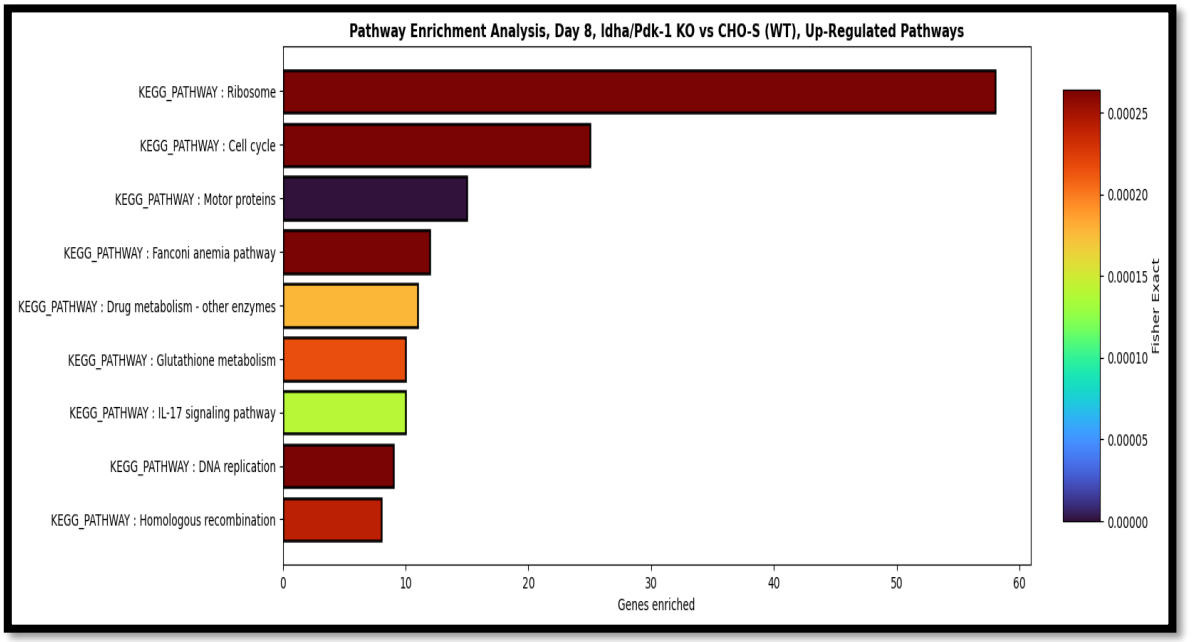

Figure 41: Stationary Phase Up-regulated pathways in LDHa/PDK-1 KO

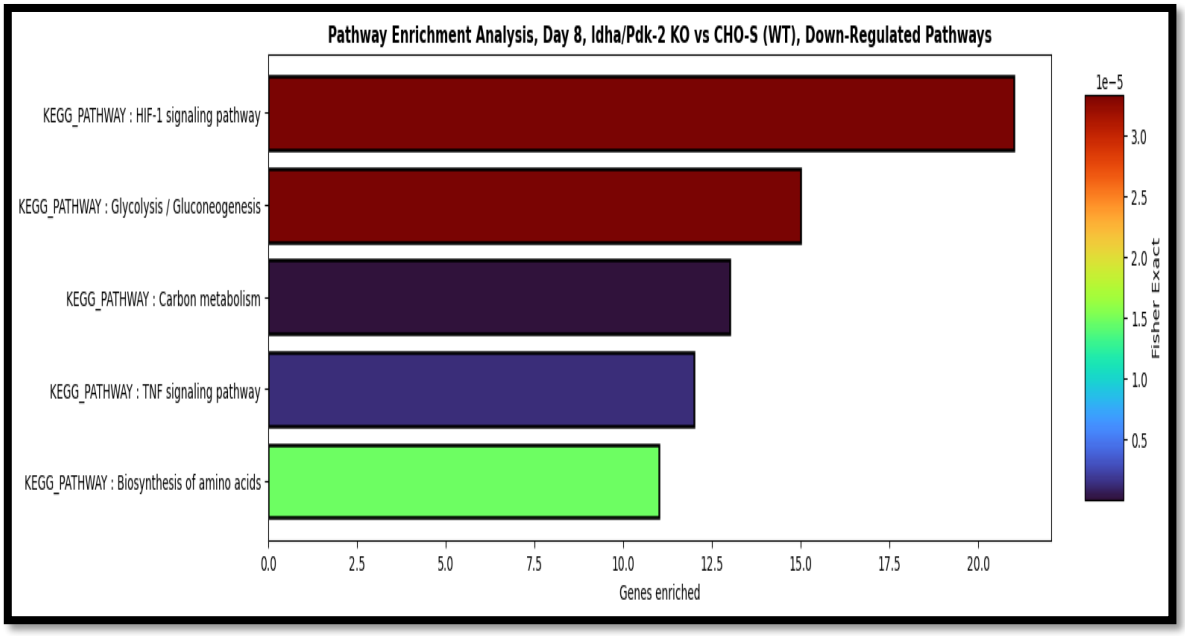

Figure 42: Stationary Phase Down-regulated pathways in LDHa/PDK-2 KO

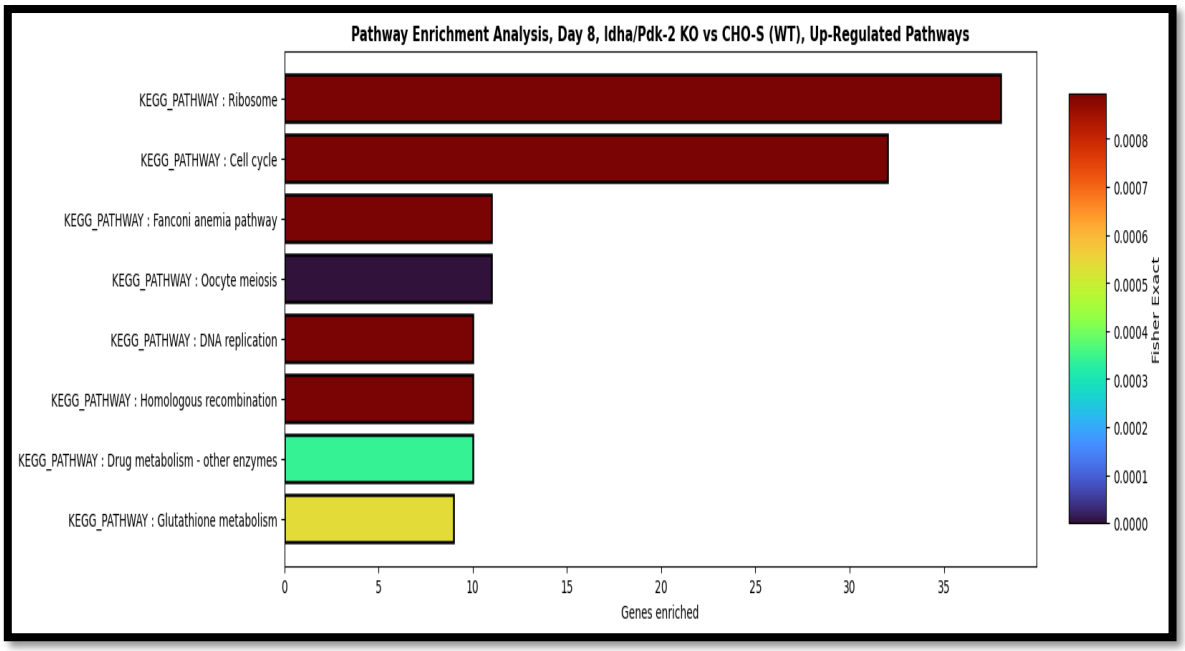

Figure 43: Stationary Phase Up-regulated pathways in LDHa/PDK-2 KO

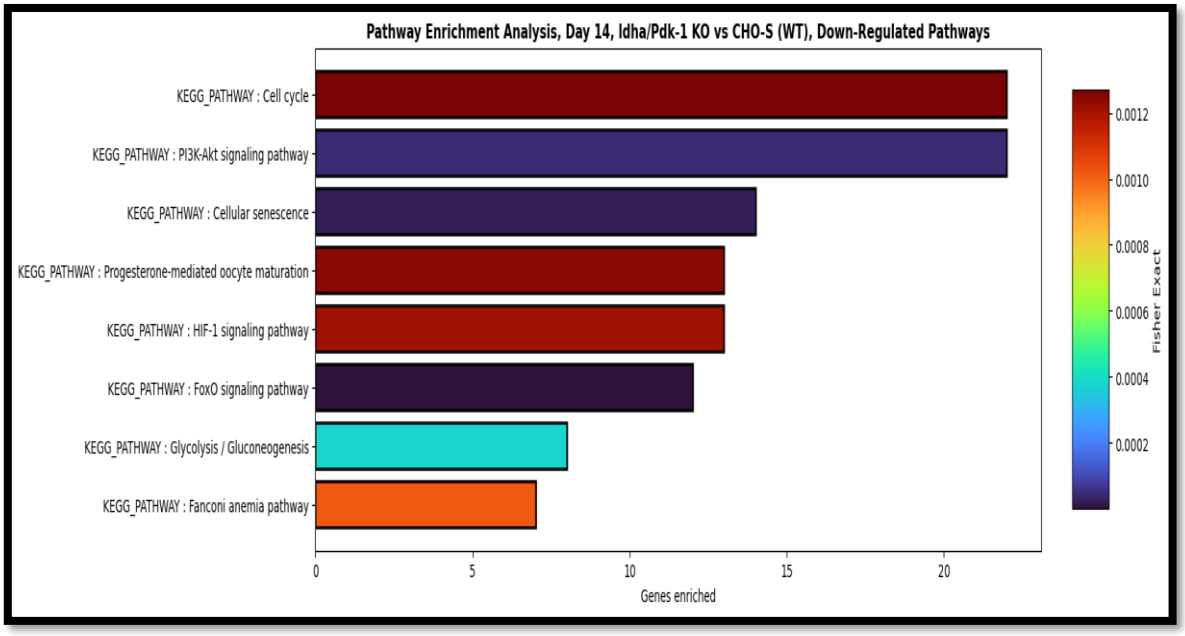

Figure 44: Death Phase Down-regulated pathways in LDHa/PDK-1 KO

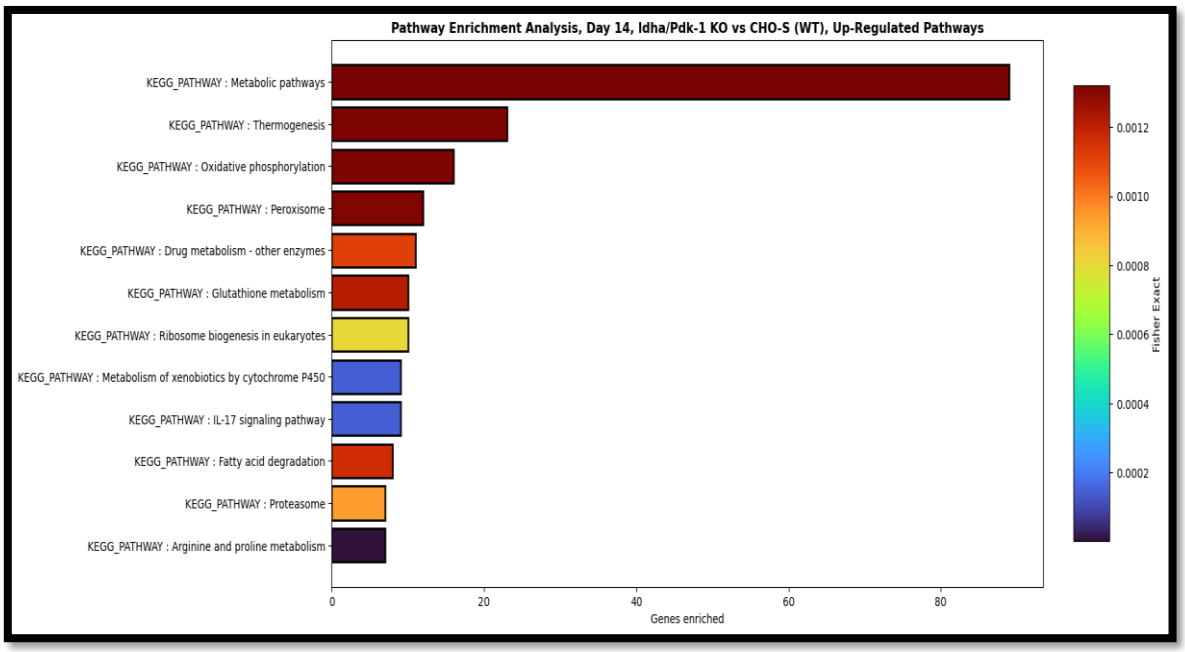

Figure 45: Death Phase Up-regulated pathways in LDHa/PDK-1 KO

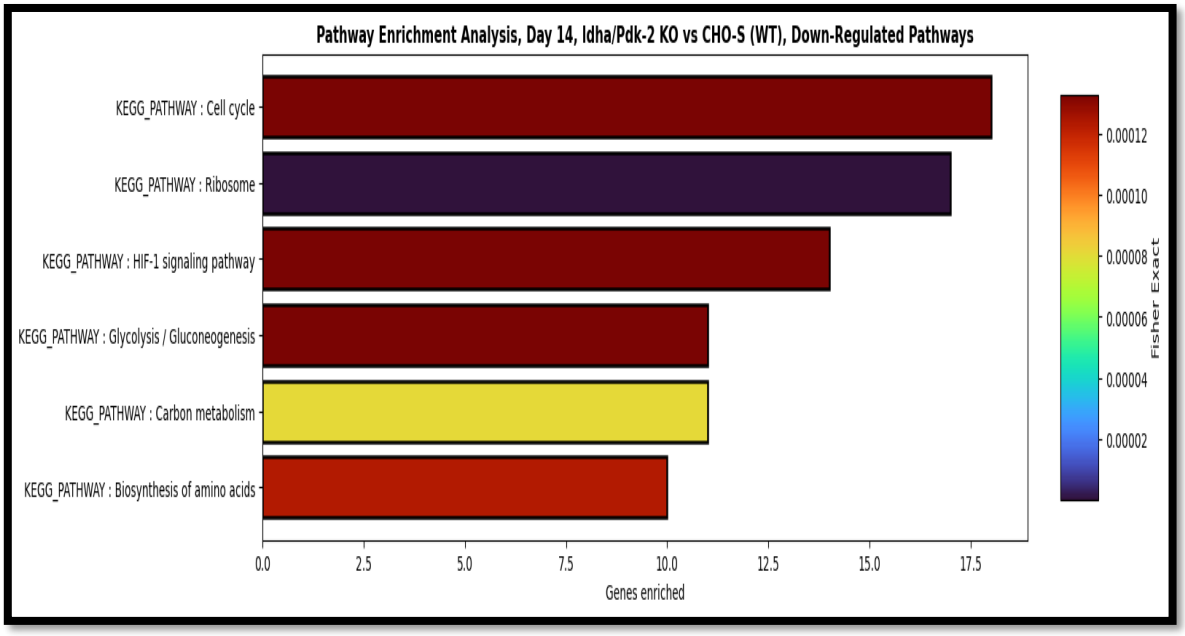

Figure 46: Death Phase Down-regulated pathways in LDHa/PDK-2 KO

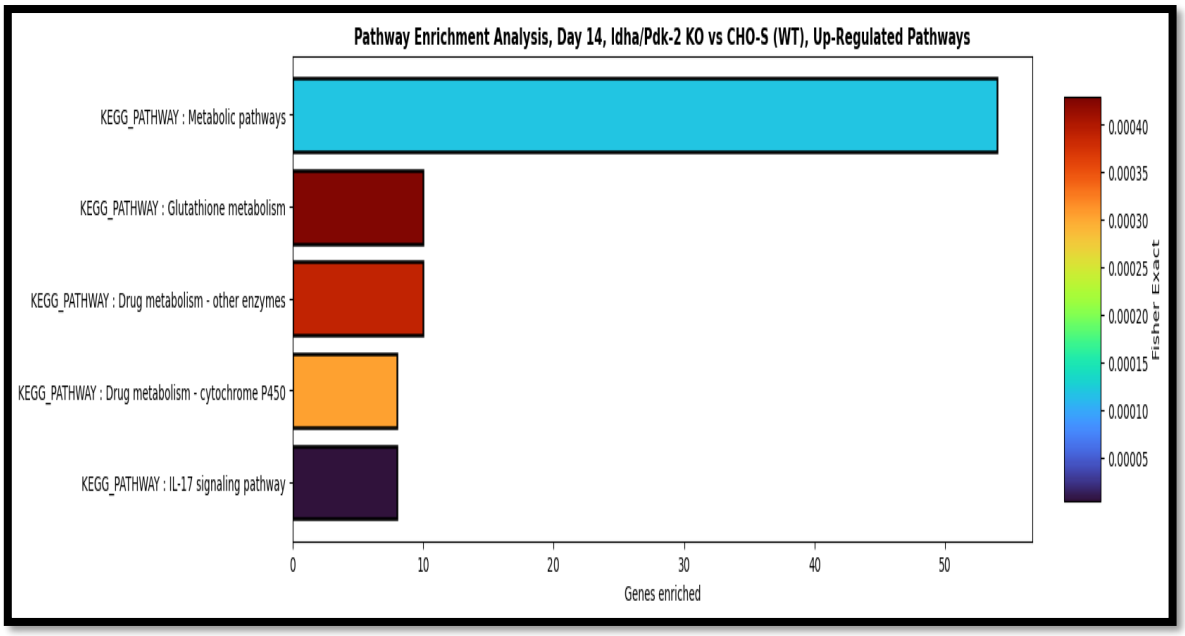

Figure 47: Death Phase Up-regulated pathways in LDHa/PDK-2 KO

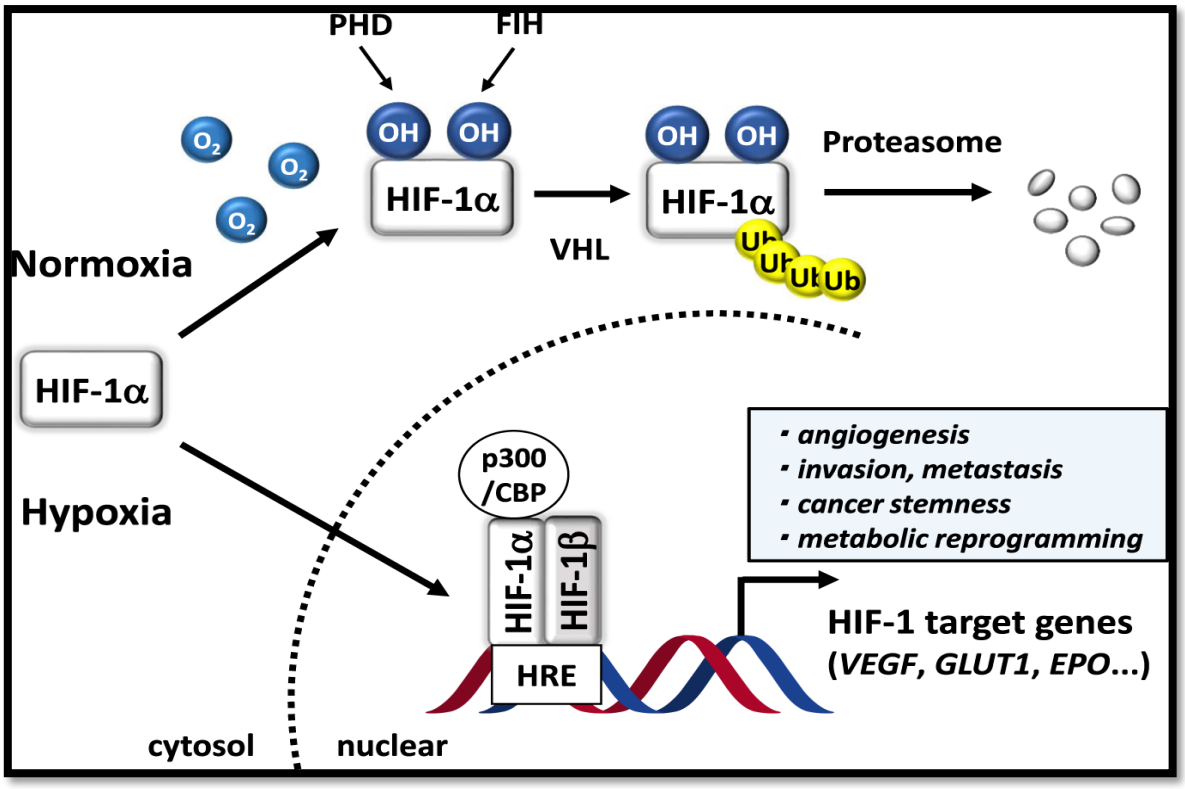

Figure 48: HIF Signaling Path

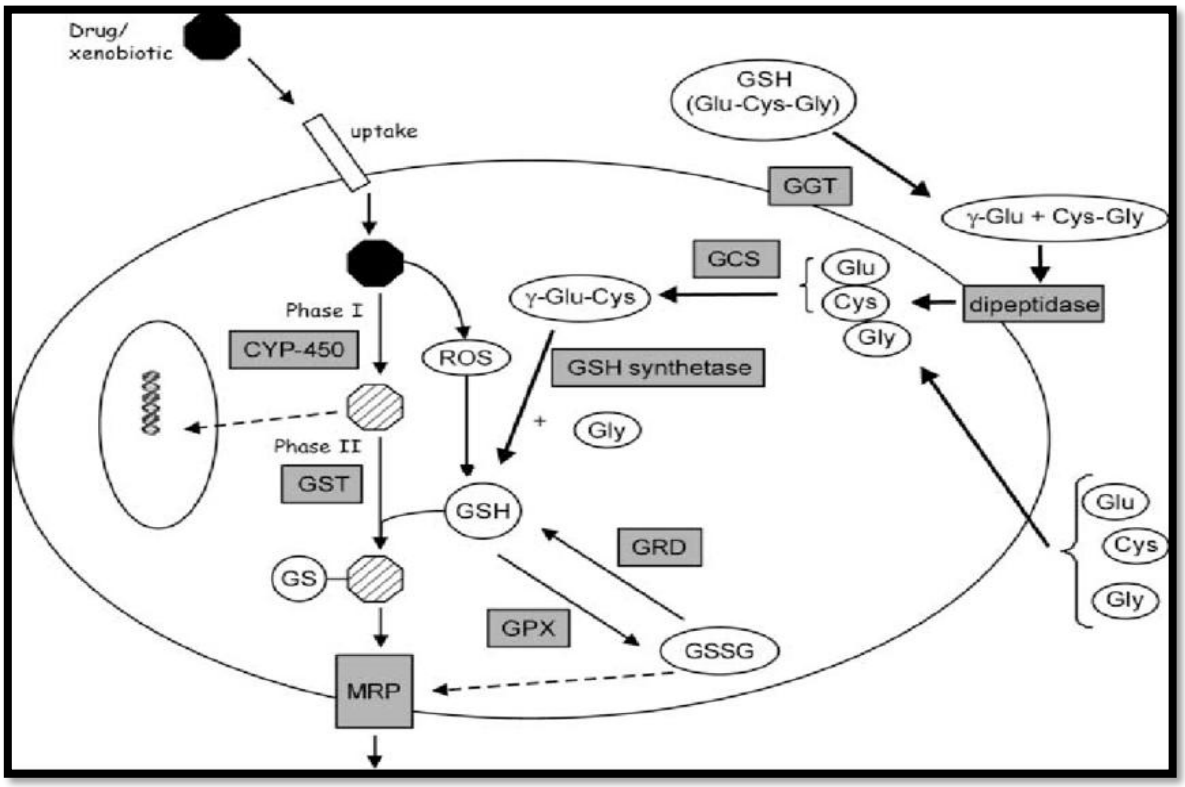

Figure 49: Glutathione Metabolism pathway

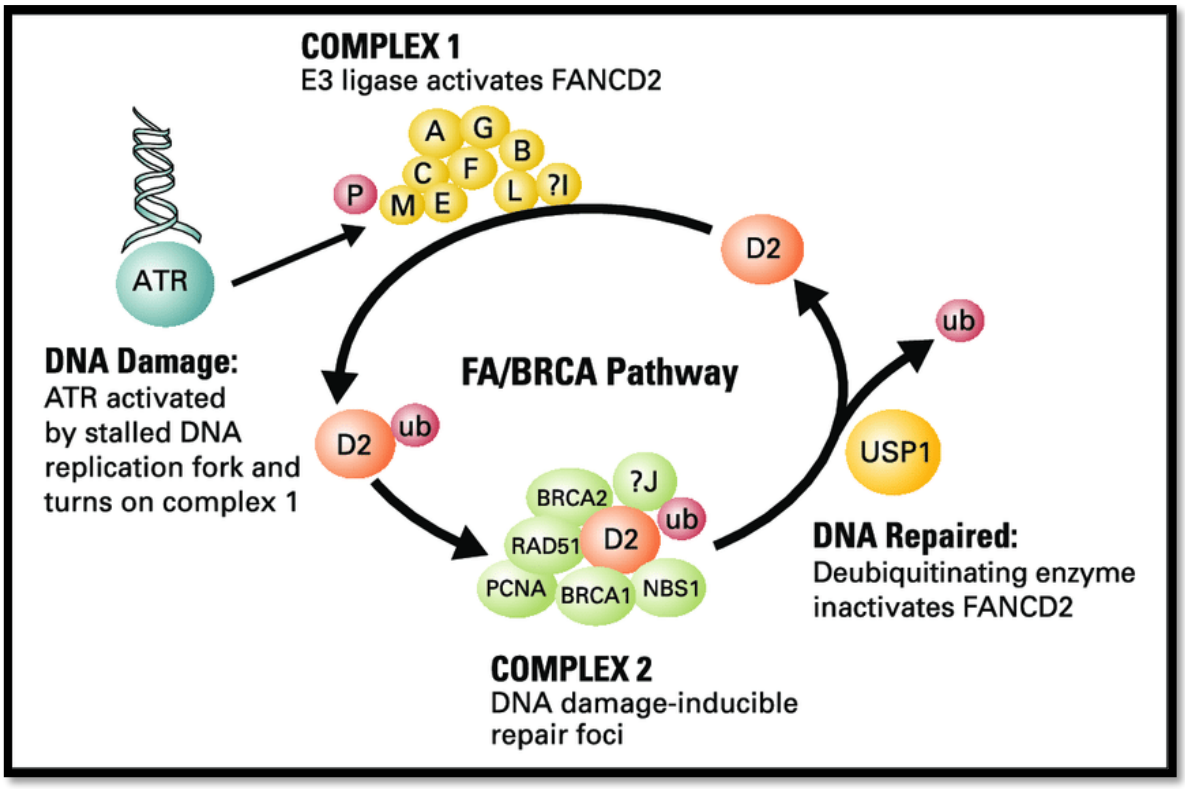

Figure 50: Fanconi Anemia pathway

S.No	Pathway	Regulation Type
1	KEGG_PATHWAY: HIF-1 Signaling Pathway	Down
2	KEGG_PATHWAY: TNF Signaling Pathway	Down
3	KEGG_PATHWAY: Ribosome	Up
4	KEGG_PATHWAY: Cell Cycle	Up
5	KEGG_PATHWAY: DNA Replication	Up
6	KEGG_PATHWAY: Glutathione Metabolism	Up
7	KEGG_PATHWAY: Fanconi Anemia pathway	Up
8	KEGG_PATHWAY: Homologous Recombination	Up

Table 2: Critical Pathways Affected in Stationary Phase (Day 8)

S.No	Pathway	Regulation Type
1	KEGG_PATHWAY: Cell Cycle	Down
3	KEGG_PATHWAY: HIF-1 Signaling Pathway	Down
4	KEGG_PATHWAY: Glycolysis / Gluconeogenesis Pathway	Down
5	KEGG_PATHWAY: Metabolic Pathways	Up
6	KEGG_PATHWAY: Glutathione Pathway	Up
7	KEGG_PATHWAY: Oxidative Phosphorylation	Up

Table 3: Critical Pathways Affected in Death Phase (Day 14)

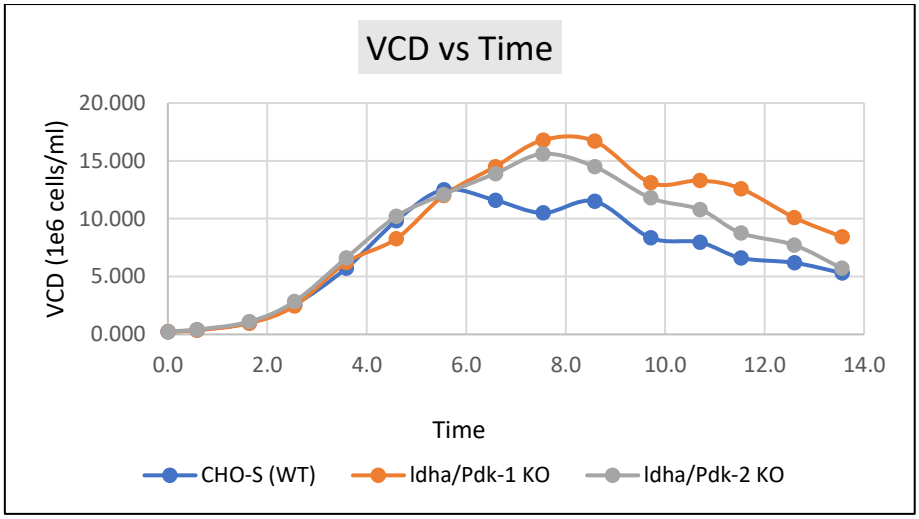

Figure 51: VCD of different cell lines vs Time

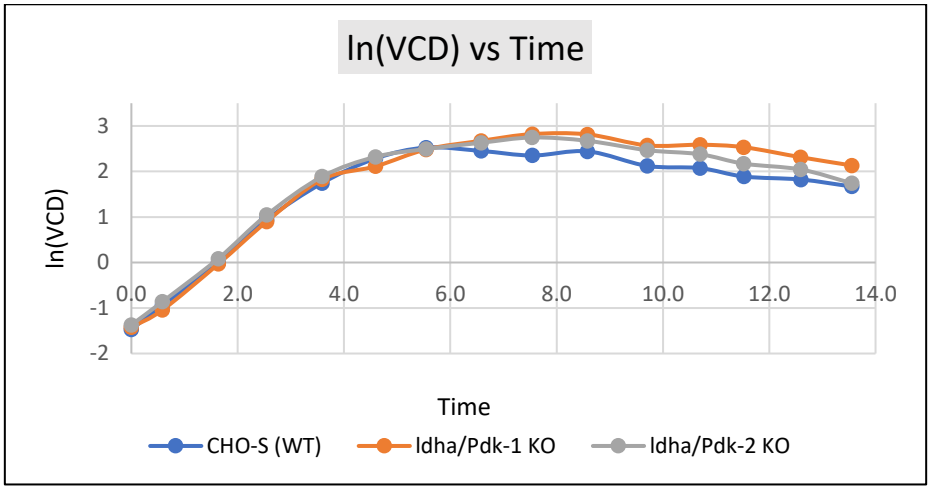

Figure 52: ln(VCD) of different cell lines vs Time

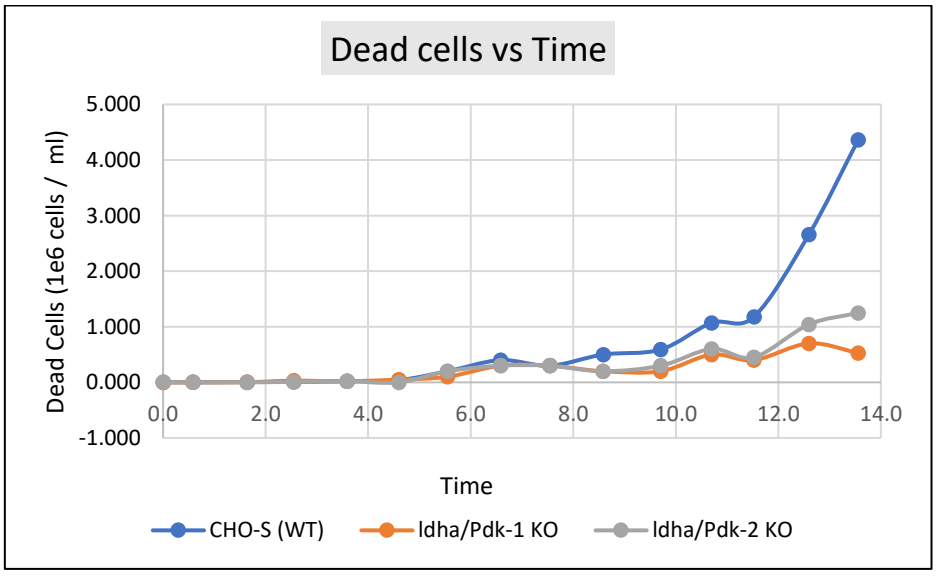

Figure 53: Dead cells of different cell lines vs Time

A note on Flux Balance Analysis (FBA)

FBA involves determining the steady state fluxes through reactions occurring in a metabolic network. FBA utilizes known stoichiometries of constituent reactions and constraints imposed on the flux values to optimize a desired objective function using different optimization techniques [4].

The iCHO2441 GEM model was used for the purposes of this project. The iCHO2441 is the most comprehensive CHO GEM available, which integrates updates to previous models regarding dead-end reactions, GPR relationships, etc. with information about protein secretory pathways. Moreover, the iCHO2441 includes the highest number of genes and genes per reaction ratio among all known existing models, thus making it a suitable choice for the integration of transcriptomics data and the subsequent FBA.

The steady state equation for different reactions in a metabolic network is given by: $S \cdot v = 0$, where S represents the stoichiometric matrix and v, the flux configuration of the metabolic network. Each element S_{ij} in the S matrix represents the stoichiometric coefficient of metabolite i in reaction j. Each element v_j in the v vector represents the flux through reaction j.

The flux values for all reactions are constrained using context-specific constraints; constraint values can be set up using calculated exchange rates, experimentally determined transcriptome data, thermodynamic constraints, etc. Here, we utilize given transcriptome data to set up constraints using the E-flux method [4].

The objective function for solving the optimization problem is also determined on the basis of the context in which the analysis is performed; for instance, the growth phase of the cells of interest. In this case, for exponential phase, the biomass reaction was used as the objective function for the exponential phase and a linear combination of the biomass and ATP maintenance reactions, with equal weights, was used as the objective function for the stationary phase. The choice of the objective function reflects the tendency of the cells to grow and divide rapidly in the exponential phase and the additional need to ensure survival in the stationary phase owing to accumulation of toxic by-products like lactate and ammonia [4].

Thus, the linear optimization problem to solve for optimum specific growth rate can be cast as:

$$max\ c^T v$$

$$subject\ to\ S \cdot v = 0,$$

$$v_L \leq v \leq v_H$$

The row vector c represents the coefficients of the metabolites involved the reaction of interest used as the objective function.

The E-flux method was used to integrate transcriptome data to set up constraint values for reaction fluxes as follows:

$$v_H = f(expression\ values\ of\ genes\ associated\ with\ the\ reaction)$$

For each reaction catalyzed by a complex requiring multiple genes, v_H was set as the minimum of the expression of the multiple genes (the ‘AND’ functionality in GPR relationships), and for reactions which can be catalyzed by one of multiple genes, v_H was set as the sum of their expression values (the ‘OR’ functionality in GPR relationships) [4]

The lower bounds of irreversible reactions were kept unchanged from the ones in the GEM (to allow for the biologically irreversible nature of the reaction built into the model), while the lower bounds of reversible reactions were updated with a value having the same magnitude but opposite sign as the upper bound, to allow for a truly irreversible reaction.

Constraint values were explicitly set up for exchange reactions to reflect differences in metabolite uptake in the exponential and stationary phases.

Flux values were scaled by a factor of 10 owing to the differences between units used for expression values (TPM) and those used for reaction fluxes ($mmol \cdot gDCW^{-1} \cdot h^{-1}$).

We aimed to perform FBA for WT and KO cell lines using transcriptome data obtained from exponential and stationary phases to observe and analyze changes in the fluxes through key reactions in the Glycolysis, Lactate Production and TCA Cycle pathways in response to the knock-out of genes whose protein products are involved in directing the Pyruvate flux either to the TCA Cycle or Anaerobic Respiration via Lactate Formation.

Google Drive:
https://drive.google.com/drive/u/1/folders/1Dorg_hEb4ziKf7_otuXLCcJPnVGoPqZs

References:

1. Hartley F, Walker T, Chung V, Morten K. Mechanisms driving the lactate switch in Chinese hamster ovary cells. Biotechnol Bioeng. 2018 Aug;115(8):1890-1903. doi: 10.1002/bit.26603. Epub 2018 Apr 10. PMID: 29603726.
2. Sheikh K, Förster J, Nielsen LK. Modeling hybridoma cell metabolism using a generic genome-scale metabolic model of Mus musculus. Biotechnol Prog. 2005 Jan-Feb;21(1):112-21. doi: 10.1021/bp0498138. PMID: 15903248.
3. Strain B, Morrissey J, Antonakoudis A, Kontoravdi C. How reliable are Chinese hamster ovary (CHO) cell genome-scale metabolic models? Biotechnol Bioeng. 2023 Sep;120(9):2460-2478. doi: 10.1002/bit.28366. Epub 2023 Mar 18. PMID: 36866411; PMCID: PMC10952175.
4. Colijn C, Brandes A, Zucker J, Lun DS, Weiner B, Farhat MR, Cheng TY, Moody DB, Murray M, Galagan JE. Interpreting expression data with metabolic flux models: predicting Mycobacterium tuberculosis mycolic acid production. PLoS Comput Biol. 2009 Aug;5(8):e1000489. doi: 10.1371/journal.pcbi.1000489. Epub 2009 Aug 28. PMID: 19714220; PMCID: PMC2726785.
5. Ebrahim A, Lerman JA, Palsson BO, Hyduke DR. COBRApy: COnstraints-Based Reconstruction and Analysis for Python. BMC Syst Biol. 2013 Aug 8;7:74. doi: 10.1186/1752-0509-7-74. PMID: 23927696; PMCID: PMC3751080.
6. B.T. Sherman, M. Hao, J. Qiu, X. Jiao, M.W. Baseler, H.C. Lane, T. Imamichi and W. Chang. DAVID: a web server for functional enrichment analysis and functional annotation of gene lists (2021 update). *Nucleic Acids Research*. 23 March 2022. doi:10.1093/nar/gkac194. [PubMed]
7. Huang DW, Sherman BT, Lempicki RA. Systematic and integrative analysis of large gene lists using DAVID Bioinformatics Resources. Nature Protoc. 2009;4(1):44-57. [PubMed]